JOINT EUROPEAN TORUS

JET–P(92)95

M.G. von Hellermann, W.G.F. Core, J. Frieling, L.D. Horton, R.W.T. Konig,
W. Mand1, H.P. Summers and JET Team

Observation of Alpha Particle Slowing Down Spectra in JET Helium Beam Fuelling and Heating Experiments

Observation of Alpha Particle Slowing Down Spectra in JET Helium Beam Fuelling and Heating Experiments

M.G. von Hellermann, W.G.F. Core, J. Frieling[1], L.D. Horton, R.W.T. Konig, W. Mand1[2], H.P. Summers and JET Team*

JET-Joint Undertaking, Culham Science Centre, OX14 3DB, Abingdon, UK

[1]AMOLF, Amsterdam, The Netherlands
[2]IPP Garching, Germany
** See Annex*

Preprint of Paper to be submitted for publication in
Plasma Physics and Controlled Fusion

ABSTRACT.

First experimental results are reported of anisotropic slowing-down features observed in JET helium beam fuelling experiments. Two independent observation ports, one with a view perpendicular to the magnetic field in the centre of the plasma, and ·a second multi-chord viewing arrangement, approximately tangential to the toroidal field, provide radially and temporally resolved information on the velocity distribution function comprising the populations of both fast and thermalised alpha particles. The fuelling process is characterised by a change-over from a distinctly non-Maxwellian distribution function to a dominantly Maxwellian distribution and also by a broadening of the deduced fast ion density radial profile. The fast particle component in the observed composite charge exchange spectrum is found to be in excellent agreement with predictions which are based on anisotropic velocity distribution functions obtained from the analytical solution of the neutral injection Fokker Planck equation.

Absolute particle densities of both slowing-down and thermalised alpha particles are determined and compared to densities and particle numbers expected from beam current and fuelling time. Thus quantitative data consistency is established for alpha particles from thermal energies up to the $^{3}He^{0}$ injection energy of 150keV. Sawtooth oscillations in both thermal and non-thermal alpha particle densities are found in low-power, low-temperature plasmas with no additional RF heating and with sawteeth periods comparable to the slowing-down time.

Signal-to-noise levels in the measurement of fast alpha particles in the JET helium fuelling campaign are extrapolated to thermo-nuclear fusion alpha particle density levels expected for the D-T phase of JET. It is shown that beam penetration and not competing continuum radiation is a major constraint, and that acceptable (hydrogen or helium) neutral beam power and energy requirements promise a feasible ex alpha particle diagnosis in the core of next-step devices such as ITER.

Introduction

The production of thermo-nuclear alpha particles and the control of the helium ash content is one of the central topics in present and next-step fusion devices (cf. POST 1991). The diagnosis of alpha particles at their birth energy and, in the subsequent slowing-down process, the radial distribution of thermalised alpha particles, are therefore of considerable interest . Numerous active and passive diagnostic techniques cover different parts of the energy spectrum, although with quite distinctive differences in their respective capabilities of energy resolution, spatial resolution and measurement of absolute particle numbers (c.f. YOUNG, 1992).

JET has recently completed a comprehensive study of the atomic physics involved in active beam based charge exchange recombination spectroscopy of alpha particles (VON HELLERMANN et al., 1991a, SUMMERS et al. 1992). The main emphasis of the present paper is the presentation of first experimental results on non-thermal alpha particles as well as the establishment of a link to absolute measurements of thermal alpha particles in a tokamak, ranging from pure helium calibration discharges to helium beam fuelling experiments and further to the investigation of slowing-down alpha particles up to energies of 150 keV. Data consistency checks in terms of absolute particle numbers, derived ion temperature, bulk plasma rotation, and energy distribution functions observed under controlled fuelling conditions are indispensable for any of the proposed next-step techniques. This refers in particular to cross-calibration techniques in fusion devices where in-situ calibrations are either impossible or become unreliable in the course of extended operation periods.

In the last experimental campaign JET has carried out helium heating experiments (c.f. MARCUS et al., 1992) using $^3He^0$ beams with energies up to 145 keV and neutral beam powers of up to 12 MW. Neutral He beam injection provides a well defined source of centrally deposited helium enabling the investigation of fuelling, heating and confinement properties. The injection leads to a population of fast ions with energies from above thermal up to the injection energy. The distribution function of the fast particles is strongly anisotropic at the birth energy but subsequently isotropises in the course of the slowing-down process. For the description of the fast ion velocity distribution function we use either an analytical solution of the neutral injection Fokker Planck equation (c.f. CORE 1991), or alternatively a time dependent comprehensive numerical solution for the entire energy spectrum including thermal particles (WOLLE et al., 1992).

The charge exchange process between fully ionised alpha particles and the neutral helium beam leads to an emission of a broad-band spectrum representing fast and thermal particles. A parametrised functional form of the predicted CX spectrum, which is a convolution of the velocity distribution function and the collision energy

dependent CX cross-sections, is used in the spectral analysis. The fit procedure is a complex coupled parameter fit which makes use of atomic predictions and which couples established parameters of the various spectral components. The number of free fit-parameters is thereby significantly reduced and the iterative procedure of a the non-linear least square fit systematically improved (c.f. MANDL, 1991, FRIELING, 1992). The absolutely calibrated CX spectrum can be used for the deduction of local fast and thermal densities and the comparison of predicted and measured spectrum provides ultimately a consistency check of the assumed slowing-down function and its parameters.

Finally we address the feasibility of thermo-nuclear alpha particle detection in the energy range up to 160 keV based on the present experimental results and its extrapolation to the future D-T phase of JET and also next-step device such as ITER. The power levels in the JET helium beam fuelling experiments exceed the expected levels of thermo-nuclear alpha particle power in the anticipated D-T phase by a factor of 5 to 10. The present helium beam fuelling experiments should however, not only enable an accurate extrapolation in signal-to-noise expectations based on actual detection efficiencies and measured continuum noise levels, but also a simulation of well defined central sources and a comparison of predicted and measured distribution functions.

Experimental layout

The experimental layout of the JET charge exchange diagnostic has been described in several earlier papers (e.g. BOILEAU et al. 1989, WEISEN et al. 1989, VON HELLERMANN et al., 1991a), but we repeat in Fig.1 the general layout of viewing lines and neutral beam injection box. It should be emphasised that for a consistent treatment of the neutral beam attenuation calculation procedure, all of the impurities contributing to the attenuation process (see also Fig.2 and Fig.3) have to be taken into account (cf. VON HELLERMANN 1991b, VON HELLERMANN 1992), and therefore all impurities need to be monitored simultaneously for accurate alpha particle slowing-down studies. The neutral beam system has two groups of identical injectors on opposite octants of the JET torus, both can be operated independently at different energies, beam powers, and operated with either hydrogen, deuterium or helium (120 keV $^4He^0$ and 145 keV $^3He^0$ respectively).

We treat in the following two different viewing arrangements (see Fig.4 and Fig.5) which are characterised by distinctively different spectra and hence interpretation procedures. The first, denoted as the **'perpendicular-view'**, is an observation perpendicular to the magnetic field, where the point of observation is a top-port of the

JET torus, and the vertical line of sight intersects the neutral beams nearby the magnetic axis. The second configuration, the 'parallel-view', describes an observation system which consists of several viewing chords in the mid-plane of the JET torus intersecting the neutral beam at 12 radial points between plasma boundary and plasma centre. In this case the observation is approximately parallel to the magnetic field and the angles between line of sight and neutral beam direction vary between 120°(plasma centre) and about 150° (plasma boundary). The initial pitch angle between neutral beam and magnetic field varies from 47° at the plasma centre to 64° at the boundary.

Spectral analysis

The presence of beryllium in most of the JET plasmas requires a simultaneous treatment of Be and He CX features in the same spectral range caused by the wavelength coincidence of the BeIV (n= 8-6) and the HeII (n=4-3) transition at λ =4686Å (see Fig.6). The problem has been solved successfully by a coupled-parameter fit procedure, which makes use of known intensity ratios and wavelength separations both in the passive boundary features and active CX plasma core spectra (cf. FRIELING 1992). For example, the CIII triplet boundary emission at 4647 Å, is characterised by a fixed intensity ratio of 5:3:1, a known wavelength separation (4647.42 Å, 4650.25 Å and 4651.47 Å), and the same ion temperature for its three components. Three parameters are therefore sufficient to fix wavelength position, intensity and temperature. In the case of the two BeIV spectra at 4658.5Å (n=6-5) and 4685.2Å (n=8-6) respectively, theoretical and beam modulation experiments have established the ratio of the effective emission rates to be 5.5 (cf. SUMMERS et al. 1991), finally the same ion temperature is assumed for all CX features. For the 'parallel-view' there is essentially a common Doppler shift of both BeIV and HeII representing the bulk plasma toroidal rotation.

It should be noted that in the analysis of the 'perpendicular-view' HeII spectrum the second passive boundary CX component (see Fig.6) , the 'luke-warm' component, can reach values of up to 2 keV in low-density, high-power plasmas with typically very high ion temperature pedestals (cf. WEISEN et al. 1991). The origin of this second, passive boundary emission feature is the CX process between a low temperature, but high density neutral hydrogen layer between separatrix and vessel wall, and fully stripped helium.

The occurrence of this additional feature has a distinctive effect on the extracted values of the actual active core CX data (see also BOILEAU et al. 1989, BURRELL et al. 1990). Similar 'luke-warm' features do exist for most of the known CX spectra (CVI , @5290.5Å, HI, @6561Å etc.). The relative intensity of the 'luke-warm' component

depends strongly on the neighbourhood of the line of sight to recycling areas in the vessel. For example for the JET 'equatorial view' the lines of sight hit the vessel wall in the torus mid-plane which is the farthest point from the recycling areas at the top and bottom of the machine in the neighbourhood of the magnetic X-points, and the luke-warm components of CVI and HeII emissions can usually be ignored.
In addition to the thermal CX spectra of HeII and BeIV (see Fig.6, 'perpendicular-view', and Fig.8 'parallel-view'), a broad pedestal, representing the slowing-down non-thermal particles, is observed during helium beam injection. In the case of the 'perpendicular-view' the pedestal has a full width of approximately $\Delta\lambda_{perpendicular} = 2 \cdot \lambda_0 \cdot v_{beam} / c \approx 90A$ and is symmetric with respect to the centre wavelength at 4686Å. In the case of the 'parallel-view' the observed observed spectra are asymmetric due to a distinctive cross-section effect, which implies that fast particles moving toward the observer (blue shift) experience a significantly reduced collision energy, whereas fast particles which move in the opposite direction can reach collision energies much above the beam energy and also the maximum for effective emission rates.

Simulation of thermal and slowing-down charge exchange spectra

The principle procedures of cross-section effects on observed spectral line shapes, and in particular on the slowing-down function of alpha particles, have been described in earlier papers (VON HELLERMANN et al., 1987, HOWELL et al. 1988, VON HELLERMANN et al., 1991a). In this paper we repeat the main steps but make use of a parametrised emission rate function and we apply the procedure on an anisotropic slowing-down function. We calculate the expected CXRS spectrum produced by slowing-down alphas by evaluating the integral:

$$f_{obs}(v_z) = \int_0^\infty v'^2\, dv' \int_0^\pi d\theta' \sin\theta' \int_0^{2\pi} d\varphi'\, g_{slow}(v', \theta', \varphi') Q_{cx}(v_r) \delta(v_z - v' \cos\theta')$$

where g_{slow} is the slowing-down distribution function, $Q_{CX} = \sigma(v_r) v_r$ the effective CX emission rate, v_r (v',v_b) the collision velocity between alpha and beam particle , and θ the angle between viewing line and v'. As a test slowing-down function we use the anisotropic function obtained from the analytical solution of the neutral injection Fokker-Planck equation (CORE, 1991), where $\xi_0 = \cos\psi_0$ is the initial pitch, v_b , v_c are the injection and critical velocity respectively, τ_s is the Spitzer slowing-down time, S is the beam deposition rate, $\beta = m_i Z_{eff} / 2m$, where m_i , m are the plasma and beam ion mass respectively. The angles in observation frame θ and φ, as well as the injection angle δ, and pitch angles ψ and ψ_0 are defined in Fig.5 . The direction of

observation is in positive z-direction, and the two solutions of the δ-function refer to particles moving either away or toward the observer:

$$g_{slow}(v,\xi)=\frac{S\tau_s}{v^3+v_c^3}\frac{1}{\sqrt{4\pi\alpha}}\exp\{-\frac{(\xi-\xi_0)^2}{4\alpha}\}$$

$$\alpha(v)=\frac{\beta}{3}(1-\xi_0^2)\log\frac{[1+(v_c/v)^3]}{[1+(v_c/v_b)^3]}$$

The slowing-down time for alpha particles determined by collisions with the background plasma is given by:

$$\tau_s=\frac{3\pi^{3/2}\varepsilon_0}{e^4\ln\Lambda}\frac{m_e m_\alpha}{n_e Z_\alpha^2}\left(\frac{2T_e}{m_e}\right)^{3/2}$$

Assuming the Coulomb logarithm $\ln\Lambda=24-\ln\{\frac{\sqrt{n_e(cm^{-3})}}{T_e(eV)}\}$ to be of the order 17 we obtain:

$$\tau_s(^3He^{2+})(sec)\approx 0.0885\cdot T_e^{3/2}(keV)/n_e(10^{19}m^{-3})$$

The critical velocity is defined by (cf. CORE 1989):

$$v_c^3=\frac{3}{4}\sqrt{\pi}\left(\frac{2T_e}{m_e}\right)^{3/2}\sum_j\frac{n_j}{n_e}Z_j^2\frac{m_e}{m_j}$$

where the indices j refer to all plasma ions. We solve the integral in three steps, first the integration in v' space making use of the properties of the δ-function, and then the integration in θ and φ. We make use of a generalised form of the δ-function:

$$d(f(x))=\sum_i\frac{1}{\left|\frac{df(x_i)}{dx}\right|}\delta(x-x_i)$$

Where the x_i are the zeros of the function f, which are in our case defined by $v'=\frac{v_z}{\cos\theta'}$

$$f_{obs}(v_z)=\int_0^\infty dv'\int_0^{2\pi}d\varphi\int_0^{\pi/2}d\theta'\frac{\sin\theta'}{|\cos\theta'|}v'^2\,g_{slow}(v',\theta',\varphi')Q(v_r)\delta(v'-\frac{v_z}{\cos\theta'})$$

For clarity we split up the resulting integral into two parts, one for particles moving towards the observer, $v_z>0$ and $\cos\theta>0$ and one for particles moving away from the observer, $v_z<0$ and $\cos\theta<0$:

$$f_{obs}(v_z, v_z \geq 0) = v_z^2 \int_0^{2\pi} d\varphi' \int_0^{\pi/2} d\theta' \frac{\sin\theta'}{\cos^3\theta'} g_{slow}\left(\frac{v_z}{\cos\theta'}, \theta', \varphi'\right) Q\left(v_r\left(\frac{v_z}{\cos\theta'}, \theta', \varphi'\right)\right)$$

and

$$f_{obs}(v_z, v_z < 0) = -v_z^2 \int_0^{2\pi} d\varphi' \int_{\pi/2}^{\pi} d\theta' \frac{\sin\theta'}{\cos^3\theta'} g_{slow}\left(\frac{v_z}{\cos\theta'}, \theta', \varphi'\right) Q\left(v_r\left(\frac{v_z}{\cos\theta'}, \theta', \varphi'\right)\right)$$

Note that the observed Doppler shift $\Delta\lambda = -\lambda_0 v/c$ is negative for particles moving toward the observer.

We have chosen a co-ordinate system which is applicable for both 'parallel' and 'perpendicular' view. It has its z-axis into the direction of observation and the neutral beam direction lies in the y-z plane (Fig. 5). In the case of the observation direction perpendicular to the magnetic field the angle $\beta_h = 90°$ and hence $\cos\beta_h = 0°$. For the JET 'parallel-view' (equatorial system) both angles β_h and β_v are small and of the order 5° to 15°.

The components of beam velocity, alpha particle and magnetic field in x-y-z and r-θ-φ frame respectively are:

$$v_{bx} = 0 \qquad v_{\alpha,x} = v_\alpha \sin\theta\cos\varphi \qquad B_x = B_t \sin\beta_v$$
$$v_{by} = v_b \cos\delta \qquad v_{\alpha,y} = v_\alpha \sin\theta\sin\varphi \qquad B_y = B_t \cos\beta_v \sin\beta_h$$
$$v_{bz} = v_b \sin\delta \qquad v_{\alpha,z} = v_\alpha \cos\theta \qquad B_z = B_t \cos\beta_v \cos\beta_h$$

the pitch angles between magnetic field and alpha particle are :

$$\cos\psi_0 = \cos\beta_v \sin\beta_h \cos\delta + \cos\beta_v \cos\beta_h \sin\delta$$
$$\cos\psi = \sin\theta\cos\varphi\sin\beta_v + \sin\theta\sin\varphi\cos\beta_v \sin\beta_h + \cos\theta\cos\beta_v \cos\beta_h$$

where ψ_0 is initial pitch angle between injection velocity vector v_b and magnetic field, and ψ the angle of the alpha particle in the subsequent scattering and slowing down process. The collision velocity v_r between alpha particle and neutral beam particle is in both viewing frames identical, and is given by:

$$v_r^2 = (v_{bx} - v_{\alpha x})^2 + (v_{by} - v_{\alpha y})^2 + (v_{bz} - v_{\alpha z})^2$$
$$v_r^2 = (v_\alpha \sin\theta\cos\varphi)^2 + (v_b\cos\delta - v_\alpha \sin\theta\sin\varphi)^2 + (v_b\sin\delta - v_\alpha\cos\theta)^2$$
$$v_r^2 = v_\alpha^2 + v_b^2 - 2v_\alpha v_b(\cos\delta\sin\theta\sin\varphi + \sin\delta\cos\theta)$$

The collision velocity v_r is used in the actual integral at $v_\alpha = v_z/\cos\theta$. In the case of the 'parallel' viewing system the observed thermal spectrum is Doppler shifted because of the toroidal bulk plasma rotation caused by the neutral beam injection. The thermal velocity distribution function is:

$$g_{thermal}(\bar{v}) = \frac{1}{\pi^{3/2} v_{th}^3} \exp\{-(|\bar{v} + \bar{v}_{rot}| / v_{th})^2\}$$

$$v_x = v_\alpha \sin\theta\cos\varphi + v_{rot}\sin\beta_v$$
$$v_y = v_\alpha \sin\theta\sin\varphi + v_{rot}\sin\beta_h\cos\beta_v$$
$$v_z = v_\alpha \cos\theta + v_{rot}\cos\beta_h\cos\beta_v$$
$$v^2 = v_\alpha^2 + v_{rot}^2 + 2v_\alpha v_{rot}(\sin\theta\cos\varphi\sin\beta_v + \sin\theta\sin\varphi\sin\beta_h\cos\beta_v + \cos\theta\cos\beta_h\cos\beta_v)$$

Where the alpha particle velocity used in the integral is at $v_\alpha = v_z/\cos\theta$.

Parametric description of the effective emission rates

In order to speed up the numeric integration procedures we approximate the discrete set of atomic data calculated for discrete energy values (cf. VON HELLERMANN et al., 1991, $D^0+He^{+2} \rightarrow D^+ + He^{+,*}$) by an empirical function of the form:

$$Q(E_{coll} = \frac{1}{2} M_p v_{rel}^2) = Q_0 \frac{(E/E_m)^\alpha}{1+(E/E_m)^\beta}$$

For the He(n=4 to n=3) transition we obtain in the case of a neutral hydrogen beam or a neutral helium beam respectively acting as a donor:

$H^0 + He^{2+} \rightarrow H^+ + He^{+,*}(n = 4,3)$

$Q_0 = (9.2 \pm 0.2)10^{-9}\,cm^3\,sec^{-1}$
$E_m = (37.0 \pm 1.7)\,keV/amu$
$\alpha = 2.26 \pm 0.19$
$\beta = 4.62 \pm 0.15$

$He^0 + He^{2+} \rightarrow He^+ + He^{+,*}(n = 4,3)$

$Q_0 = (4.6 \pm 0.1)10^{-9}\,cm^3\,sec^{-1}$
$E_m = (53.3 \pm 3.1)\,keV/amu$
$\alpha = 2.42 \pm 0.23$
$\beta = 4.02 \pm 0.14$

Fig.2 illustrates the empirical fit to the effective emission rates which are calculated for a standard JET plasma with a density of $n_e = 3 \cdot 10^{19} m^{-3}$, T=10keV and $Z_{eff}=2$. The term

'effective' refers to the state selective emission rate following charge capture and redistribution processes (cf. BOILEAU et al. 1989). Note that the rates are not averaged over a velocity distribution function. The maximum emission rates for a helium beam acting as a donor in the CX process are approximately half of that for a hydrogen beam. The maximum rate in the case of a neutral helium beam is shifted towards a higher collision energy due to the higher orbit velocities for the bound electrons in the helium beam.

In order to determine a particle number density representing each of the two populations in the observed composite spectrum we make use of the integrated spectral intensity defining an averaged emission rate for both thermal and slowing-down particles.

$$\langle \sigma v \rangle_{average} = \frac{\int_{-\infty}^{\infty} f_{obs}(v_z)\,dv_z}{\iiint d^3v\, g_{slow}(\bar{v})}$$

$$\langle \sigma v \rangle_{average} = \frac{\int_{-\infty}^{\infty} dv_z \int_0^{\infty} v'^2\, dv' \int_0^{\pi} \sin\theta'\, d\theta' \int_0^{2\pi} d\varphi'\, g_{slow}(v',\theta',\varphi') Q(v',\theta',\varphi') \delta(v_z - v'\cos\theta')}{\int_0^{\infty} v^2 dv \int_0^{\pi} \sin\theta d\theta \int_0^{2\pi} d\varphi g_{slow}(v,\theta,\varphi)}$$

The averaged emission rate, resulting from the integration over the entire spectrum, is slightly lower for the fast particle spectrum than that for the thermal spectrum, since the broad fast spectrum extends over a wider range of collison energies, well beyond both sides of the maximum at approxiamately 55 keV/amu. We obtain for the $^3He^0$ injection case of 45keV/amu, at a temperature of 10 keV for both 'perpendicular' and 'parallel view':

$$\langle \sigma v \rangle_{fast} = 1.62 \cdot 10^{-9} cm^3 sec^{-1}, \text{ and } \langle \sigma v \rangle_{thermal} = 1.88 \cdot 10^{-9} cm^3 sec^{-1}$$

Results

1)Comparison of modelled and observed spectra

The experimental evidence collected in the JET He beam fuelling experiments have confirmed essentially the predicted shapes of active CX spectra for thermal and non-

thermal particles. We illustrate the main characteristics by two representative sets, one for the view perpendicular to the magnetic field and also perpendicular to the neutral beam (Fig.6 to Fig.7) , and a second set collected by the 'parallel' viewing system (Fig. 8) . Fig.6 shows both thermal and non-thermal spectra in linear intensity scale and Fig.7 the same spectrum in logarithmic scale versus energy. The thermalised spectrum is in close approximation again a Gaussian, however in a Doppler shifted position and with a different width. An overview on the cross-section effects on observed Doppler-shifts, Doppler-widths and intensities has already given elsewhere (c.f. VON HELLERMANN et al., 1991[a,b] ($He^{+2} + H^0$, $C^{+6} + H^0$) and DANIELSSON et al. 1992, $C^{+6} + H^0$) .

At the beginning of the fuelling process, when the non-thermal population has a density equal to, or is even exceeding that of the thermal population, the high energy characteristics are quite obvious. This is clearly demonstrated in the first case (' perpendicular' view) where a logarithmic plot both of experimental (Fig.7a) and simulated slowing-down spectrum (Fig.7b) shows that, to a first approximation, the observed shape can be described by the above anisotropic function and evidence of a fast particle population within the discharge can be unambiguously deduced. The modelled fast particle function is strictly speaking only valid for energies ranging from the neutral beam energy to energies above thermal energies. The logarithmic presentation illustrates however clearly the distinctive onset of the fast spectrum at the injection energy, well above the background fluctuation level of continuum radiation. In principle, a comprehensive numerical treatment of the entire distribution function, as for example described by WOLLE 1992, containg a smooth transition between fast and thermal population, should be used to modell the observed spectrum.

The characteristics of the non-thermal contribution to the composite CX spectrum is even stronger in the case of the 'parallel' viewing system where the relative amplitude of the fast population not anly changes considerably in time but also over the radius. Fig.8 shows the modelled spectra for 4 different radii, located between plasma boundary and plasma centre. The changing spectral shapes reflecting primarily the anisotropy in the slowing-down function expressed by the variation of viewing angle δ and initial pitch angle ψ_0. The role of the collision energy dependent CX emission rate on the observed spectra is illustrated by overlaying the two cases of either assuming a constant cross-section for the entire energy range of observed alpha particles $Q_{cx}(E_{collision}=E_{beam})$, and in the second case using the actual $Q_{cx}(E_{collision}=f(v_{alpha},v_{beam}))$ dependence. The characteristic shapes of both thermal and non-thermal feature are essentially maintained, however with a slight Doppler shift and a modified halfwidth and intensity. This implies that the modelled slowing-down function is in a first order approximation successfully recovered.

In Fig.9 we give two representative experimental time slices, one at the beginning of the fuelling process, and the second approximately a second later. The overlapping of the two populations (Fig.9a) indicate that neither description of 'fast' or 'thermal' is adequate in the transition area ($v \approx 2v_{th}$), and that an actual 'temperature' attributed to the thermal feature is only justified in the red-wing of the spectrum where the non-thermal part is siginificantly reduced in intensity. This is markedly different for the second time slice (Fig.9b) where the thermal population is the dominant CX feature.
Note that the asymmetries of the non-thermal CX spectrum and the Doppler shift of the thermal spectrum as described in this paper are specific for the 'parallel' view and its angles δ between line of sight and neutral beams. For the divertor phase of the JET experiment the charge exchange observation system will be moved to a different octant of the JET torus with an observation looking down-stream onto the neutral beams and therefore an effective red-shift of the maximum of the fast spectrum. The main part of the non-thermal slowing-down feature will then be shifted into the line-free wing of the HeII spectrum. This fact will, in principle at least, facilitate low level alpha particle detection.

2) Thermal ion temperature and density

One of the crucial tests for the unambiguous identification of the thermal feature in the CX HeII spectrum (> 0.5 sec in the fuelling time) is the consistency of both its deduced temperature and density with complementary plasma diagnostic data. For this reason we show an example of a 'pure' helium plasma with a core electron density of $4 \cdot 10^{19} m^{-3}$ with only a moderate neutral (deuterium beam) heating power of 2 MW and both ion and electron temperature approximately the same low level of about 3 to 4 keV (Fig. 10). There is no additional RF heating and distinctive sawtooth oscillations with short periods of 200 msec are observed.
The impurity content of intrinsic impurities carbon and beryllium is in this example (JET pulse #23210) small compared to the fuelling gas content ($n_C/n_e=0.01$ and $n_{Be}/n_e=0.005$). The deduced helium density which in a 'pure' helium plasma is expected to be half of the electron density is found to reach values of about 55% of the electron density. The upper and lower values of the deduced helium density (time trace Fig.10b and radial profile Fig.10c) reflect essentially the errors in the beam attenuation code, which contain an error of 10% in either electron density or neutral beam stopping cross-sections (see also the paragraph on signal-to-noise). The injected neutral beam is in this example a deuterium beam of 80 keV. The absolute calibration is based on in situ calibration before and after operation and in addition on a cross-

calibration technique making use of several independent bremsstrahlung measurements on JET .

The second class of plasmas which was used for the assessment of CXRS based absolute alpha particle density measurements were low-density deuterium target plasmas with substantial He-beam fuelling. The low helium pumping efficiency of the graphite walls of the JET device implies that most of the fuelled particles can be recovered within the confined plasma. This enables - in principle - a further fiducial test for data consistency, which is a direct comparison of the deduced total helium content with in the entire plasma volume to the particle number derived from the neutral beam current and the fuelling time (cf. Fig.11).

A reliable deduction of the helium density, especially in the case of high neutral beam attenuation and therefore low CX signals, is further complicated by the so-called plume effect (FONCK, 1982). Hydrogen-like helium ions produced by charge exchange have a significant probability of being excited and emitting a photon before being reionised. Since, at temperatures typical of JET, these ions can stream several metres along magnetic field lines, the local nature of charge exchange measurements can be compromised. We have performed detailed calculations of the plume contribution to helium signals, including necessarily the correct JET beam, magnetic, and viewing geometry. Corrections for outer viewing chords are typically of the order 5-10% and are localised to essentially the same plasma minor radius as the initial interaction volume, due to the tangential viewing geometry. Further towards the plasma centre corrections are larger, and can, in some cases, alter the interpretation of the ion temperature profile. Similar effects have been reported in TFTR (SYNAKOWSKI, 1991).

3)Non-thermal alpha particle population

The observed broad band spectral emission may, in principle, be due to two excitation processes:

1) $He^{2+}_{fast} + He^{0}_{fast} \rightarrow He^{+,*}_{fast} + He^{+}_{fast}$ the prompt signal, and

2a) $He^{+}_{fast} + e^{-} \rightarrow He^{+,*}_{fast} + e$

2b) $He^{+}_{fast} + Z^{+z}_{thermal} \rightarrow He^{+,*}_{fast} + Z^{+z}_{thermal}$ delayed excitation.

The second process leading to a high energy plume, the only qualitative difference being that, at these high energies, ion excitation must also be considered. Several factors indicate that the CX interaction of probe neutral beam and alpha particles is indeed the dominant process. The 'fast' signal only exists when the probe beam is switched on and at least one of the neutral beam sources is injecting helium, secondly

the observed 'fast' intensities are found to be correlated to both CXRS probe beam power and the total helium fuelling rate. Thirdly the observed spectral shapes, both for 'perpendicular' and 'parallel' view, agree with the modelled charge exchange spectra, and, in particular for the second case, the prediced changes as function of viewing angle and pitch angle are recovered . The fourth, and possibly strongest evidence, is the fact that the deduced radial profiles (Fig. 12) indicate a strong peaking on-axis and subsequent collapse and accumulation nearby the q equal 1 surface during a typical sawtooth crash.

In the following we present some results of the JET helium beam heating campaign, (cf. MARCUS et al. 1992) where the broad-band fast particle spectrum was systematically assessed for the first time. The total neutral beam fuelling powers of this experimental campaign with around 200 JET pulses were typically ranging between 2 and 11 MW, and with deuterium target densities of the order 2 to $5 \cdot 10^{19}$ m^{-3}. For some of the pulses the coupling efficiency of ICRH in a ^3He minority plasma was studied applying moderate RF power levels of about 5 MW. We have selected in the following overview two representative classes. In the first class we describe low-density, high-temperature and high-power heating experiments where the injection of helium beams contributes significantly to the increase of the target electron density and to the heating process. In a second example we will show low-power, low temperature, medium density plasmas, where no RF power is applied and strong sawtooth activities can be observed.

Fig.13 gives a survey of the main plasma data for a typical hot-ion mode plasma. In the course of the fuelling and heating phase (including an ICRH power of 4 MW) both ion and electron temperatures increase and reach levels of 13 and 8 keV respectively. At the same time the thermalised minority density increases almost linearly in time (Fig. 14) , whereas the fast density remains constant, reflecting a constant source rate in a moderately changing target density. The observed fuelling rates are of the order $2 \cdot 10^{18}$ $m^{-3}sec^{-1}$, and maximum concentrations of approximately 10 to 20% of the electron density are reached in the course of the fuelling process.

If there was no recycling of helium from previous pulses we would expect in principle the thermalised population starting from a zero level, and the fast population reaching a stationary level after a equilibrium time t_{stat} (cf. WOLLE 1991, ANDERSON 1983):

$$t_{stat} = \tau_s \log[1+(v_b / v_c)^3]/3$$

Typical slowing-down times (Fig. 13d) are of the order of 0.5 to 1 sec and stationary fast particle distributions are reached within t_{stat}= 100 to 200 msec. The temporal resolution of the JET CX diagnostic is 50 msec and therefore not sufficient to establish the actual transition to equilibrium.

The radial profiles for fast ion densities (Fig.12), using in a first approximation a sum spectrum of a Maxwellian and a slow-down function, yield qualitatively a strong on-axis peaking in first few 100 msec of the fuelling process. In the course of the fuelling process the profiles broaden and become even hollow after approximately 1 sec. The apparent 'temperature' attributed to the Maxwellian part of the CX spectrum is distinctly lower (30%) than the temperature deduced from the 'perpendicular' view (see also Fig.13). Both temperatures are approximately equal at the end of the fuelling phase, when the electron density has risen to $4 \cdot 10^{19} m^{-3}$, and are comparable to the central electron temperature. We can, in principle, use the derived densities and local time scales t_{stat} to deduce local source rates.
In helium beam fuelled JET plasmas with no additional ICRH usually strong sawteeth activities can be observed. They are reflected in particular in electron and ion temperature oscillations (see also Fig.10 and Fig.15). By contrast are the sawteeth amplitudes of electron density and thermalised helium minority density relatively small. We have found for the first time distinctive oscillation in the fast ion density. Fig. 15 gives two examples with sawtooth periods of 160 and 420 msec respectively. The fast particle oscillation is found to be out of phase with that of the thermal particles. It should be noted that in a He fuelled plasma only thermal neutron production exists and the sawteeth activity in the fast ion population and the thermal-thermal neutron rate is not related . The sawtooth periods ($\approx$160 msec and 420 msec respectively) are of the same magnitude as the slowing-down time τ_s ,which is $\approx$200 msec in both examples (cf. also KOLESNICHENKO et al. 1992).

Alpha particle detection in the future D-T phase of JET

Two limiting factors for a successful CX alpha particle diagnostic depend primarily on the penetration efficiency of the probe neutral beam. The first is the detection of the active CX spectrum against the competing background spectrum. And the second factor, which is even a more general constraint, is that for a useful quantitative exploitation of the derived spectra the local neutral beam strength needs to be accurately assessed. The beam strength is usually derived from input data such as stopping cross-sections and electron density and temperature profiles. A typical error of the input data of 10% implies that due to the exponential decay of the beam strength along the penetration path into the plasma, only a maximum attenuation factor of the order 5 to 10 % of the vacuum beam density can be tolerated. Beyond this threshold attenuation errors, and therefore also errors in deduced alpha particle densities, exceed 50%.

Typical fast particle densities observed during the JET helium beam heating campaign with total powers up to 12 MW, were between $2\cdot10^{17}$ m^{-3} and $5\cdot10^{18}$ m^{-3} (cf. Fig.16), the lowest level corresponding to a detection limit with a signal/noise of 1, where the noise is defined by the ratio of measured counts from charge exchange photons divided by the fluctuations of bremsstrahlung background plus CX signal counts. The signal-to-noise ratio in an optimisation study is conveniently expressed in terms of the neutral beam current density $\mathbf{I_{neutral} = e \cdot n_{beam} \cdot v_{beam} \cdot A_{beam}}$, which is usually a fixed quantity for a given ion source. For example for negative ion beam sources (HOLMES 1992) the beam current is a constant over a wide energy range. In the case of the detection limit we may assume that the bremsstrahlung counts are exceed those of the CX signal, $N_{brems} >> N_{CX}$, we may write therefore :

$$\{\frac{S}{N}\} = \frac{N_{CX}}{\sqrt{N_{brems} + N_{CX}}} \approx \frac{N_{CX}}{\sqrt{N_{brems}}}$$

$$N_{cx,max} = \frac{\Delta\lambda}{\sqrt{\pi}\cdot\lambda_d}\Delta t\cdot\Re\cdot\frac{I_n}{\sqrt{\pi}\cdot w_\perp\cdot e}\cdot n_\alpha\cdot\sigma_{cx}\cdot\exp\{-\int dr\cdot n_e\sum_z c_z Q_z\}$$

Where we have introduced $w_\perp$ the beam width perpendicular to the line-of-sight ($A_{beam} = \pi\cdot w_\perp\cdot w_{l.o.s}$) , n_α and $c_\alpha = n_\alpha/n_e$ the alpha particle density and concentration respectively, Δt the integration time, $\Delta\lambda$ the wavelength interval, $\lambda_d = \lambda_0\sqrt{\frac{2T_i}{m_\alpha c^2}}$ the Doppler width of the CX spectrum, $\Re$ the detection efficiency ($\Re = t\cdot\eta\cdot\varepsilon$ defines the number of counts per radiance, with optical transmission t, quantum efficiency η, and ε the spectrometer étendue $\varepsilon = \Delta\Omega\cdot A_{sp}$), σ_{CX} the CX emission cross section. The neutral beam attenuation is determined by effective stopping cross-section Q_Z, including electron and ion impact ionisation as well as charge exchange processes, $c_Z = n_Z/n_e$ are the respective impurity concentrations. For the fluctuation of the free-free continuum radiation background signal we have:

$$\tilde{N}^2 = B\cdot G_{ff}\cdot Z_{eff} < n_e^2(0) > L_p\frac{\Delta\lambda}{\lambda_{de}(0)}\Delta t\cdot\Re \qquad \text{where} \qquad B = \left[\frac{e^2}{4\pi\varepsilon_0}\right]^3\frac{16}{3hc^4m_e^2}\sqrt{\frac{\pi}{3}} \quad ,$$

$\lambda_{de} = \frac{\lambda}{c}\sqrt{\frac{2T_e}{m_e}}$ an equivalent Doppler width defined by the electron velocity, G_{ff} the Gaunt factor, L_p the effective length contributing to the line-of-sight integration: $\frac{< n_e^2(0) > L_p}{T_e^{1/2}(0)} = \int ds(r)\frac{n_e^2(r)}{T_e^{1/2}(r)}$, and Z_{eff} the effective plasma ion charge. We obtain finally:

$$\{\frac{S}{N}\} = \frac{I_n c_\alpha \sigma_{CX} \exp\{-\int dr n_e \sum_z c_z Q_z\}}{\pi w_\perp e \sqrt{Z_{eff} G_{ff} L_p B}} \sqrt{\frac{c \cdot v_e}{v_\alpha^2}} \sqrt{\Delta t \frac{\Delta\lambda}{\lambda} \Re}$$

We have simplified the case by assuming either a neutral helium beam or a negative ion hydrogen beam acting as probe beam and therefore only one energy component needs to be considered. It is interesting to note, that for a fixed alpha particle concentration $c_\alpha = n_\alpha / n_e$, which is for a fusion reactor of the order 1o% (cf. POST 1991), the linear electron density dependencies in the S/N expression cancel each other, and the remaining density dependence is solely given by the beam attenuation process. For a constant alpha particle concentration is therefore the bremsstrahlung level not a limiting factor. The beam stopping is primarily determined by the beam energy. Both charge exchange cross-sections and beam stopping cross-sections have only a slight electron density dependence because of redistribution and multiple-step processes (cf. BOILEAU et al. 1989, MANDL et al. 1992). For a given electron density there is then obviously an optimum energy which is defined by the trade-off of gaining with higher energies in beam penetration but loosing at the same time by the drop of the CX emission rate.

Fig. 17 gives a survey of measured continuum levels for over 50 JET pulses, and its corresponding fluctuation levels. It illustrates that the noise in the continuum background signal follows over several orders of magnitude Poisson statistics and the theoretical S/N ratio, as defined above, is therefore justified. This implies that, at least in principle, the detectability of CX spectra can be improved by improving for example the detection efficiency of the instruments and observation optics.

In Fig. 18 we show the normalised signal-to-noise ratio ($\{S/N\}/I_n$) as a function of the line integrated electron density for the case of a neutral hydrogen and a neutral helium beam respectively. The line integrated electron density refers to the line integral along the neutral beam extending from the plasma boundary to the point of observation. For each density value in Fig. 18 and Fig.19 an optimised energy has been calculated which leads to a maximum in the S/N ratio at this density. The detection efficiency in both cases is assumed to be of the order $\Re = 5 \cdot 10^{-6} \frac{\text{counts/ sec}}{\text{photons/ cm}^2 \text{ sec sr}}$.

This corresponds to a value established for the JET CX diagnostic system of the next experimental campaign, based on back-illuminated CCD detectors with quantum efficiencies of the order 60 to 70 % at 4686 Å, and a spectrometer étendue of ε=0.006 mm^2sterad.

In the D-T phase of JET with anticipated target densities of the order 3 to $4 \cdot 10^{19}$ m^{-3} , and alpha particle powers up to 2 MW, we may expect slowing-down densities below 200 keV of the order of 1 to $2 \cdot 10^{17}$ m^{-3} , that is alpha particle concentrations of 0.5% of the electron density. Using the data displayed in Fig. 18 and 19, this would correspond to a signal-to-noise level of 5 to 10 assuming an effective neutral beam current of the order 10A contributing to the CX lines of sight. (corresponding to approximately 5 MW at 65 keV/amu for a hydrogen neutral beam, and 12 MW at 110 keV/amu for a $^3He^0$ beam..

The anticipated dimensions of the next step device ITER (International Thermo Nuclear Experimental Reactor) imply that the JET central densities have to be divided roughly by two to obtain an equivalent density level with the same S/N ratio at ITER. The beam penetration length at JET from the boundary to centre, with a tilt angle of 19.5° of the injection box, is 1.2 m compared to a penetration length of 2 m from the boundary to the centre of the machine at ITER assuming a radial injection system (cf. MUKHOVATOV et al. 1991). If we assume for ITER for example a negative hydrogen ion source neutral beam system (to reduce the beam divergence) and a neutral current of the order 50A we expect at a central electron density of $10^{20}m^{-3}$ and also $\langle n_e L \rangle_{bc} \approx 10^{20} m^{-2}$, an alpha particle density $n_{alpha}(0)=5 \cdot 10^{18} m^{-3}$, that is a 5% concentration, and a hydrogen beam energy of 100 keV/amu a signal-to-noise of 10 .

A further relevant consideration is however not only the detectability of an alpha particle slowing-down spectrum in the core of a plasma but also the quantitative deduction of a local alpha particle density from the measured CX photon flux. The error in the deduced density introduced by an error in the attenuation is for example in the case of a 100keV/amu hydrogen neutral probe beam:

$$n_\alpha = \frac{4\pi\phi_{cx}}{n_b L_{cx} \langle \sigma v \rangle_{cx}}$$

$$n_b = n_b(0) e^{-\int dr n_e \sum_z Q_z c_z}$$

$$\frac{\Delta n_\alpha}{n_\alpha} = \frac{\Delta n_b}{n_b} \approx \frac{\Delta(Q_z, n_e)}{(Q_z, n_e)} \cdot \sum_z Q_z c_z \cdot \int_{plasma-boundary}^{cx-volume} ds \cdot n_e$$

Here we have assumed a total error of 10% error in electron density n_e and stopping cross-sections Q_z. For example in a plasma with impurity ion composition (n_Z/n_e) of He^{2+}(10%), C^{6+}(2%), H^+(68%), that is an effective ion charge Z_{eff}=1.8, we have in the case of a hydrogen neutral beam with 100keV/amu a total stopping cross-section of $\Sigma Q_z c_z = 2.4 \cdot 10^{-20} m^{-2}$, with $Q_H = 1.9 \cdot 10^{-20} m^{-2}$, $Q_{He} = 5.8 \cdot 10^{-20} m^{-2}$, $Q_C = 25.2 \cdot 10^{-20} m^{-2}$. (see also Fig.3). For a line integrated electron density of $\langle n_e L \rangle_{boundary\text{-}cx\text{-}volume} = 2 \cdot$

$10^{20}m^{-2}$, this corresponds to an observation in the core of ITER at a central density of $10^{20}m^{-3}$, we would therefore expect an error of at least 50% for a hydrogen beam and approximately 20% for a helium neutral beam. The successful treatment of neutral beam penetration is therefore relevant in two respects: Detectability and reliable calculation of a local beam strength.
Beam emission spectroscopy (cf. BOILEAU et al. 1989, VON HELLERMANN and SUMMERS 1992, MANDL et al. 1992) has recently given access to a direct measurement of the neutral beam density via the Doppler shifted beam emission spectrum. By modelling of the excitation processes (ion impact excitation and to a lesser extent electron impact excitation) local densities can be derived. This new information provides an additional consistency check and - in principle - an extension of the accessible plasma density range.
A further problem on top of the competing processes of bremsstrahlung and of beam attenuation are the possible occurrences of spurious light emissions in the spectral region around the 4686 Å wavelength regime, caused for example by the exposure of optical fibres to enhanced neutron bombardement or gamma radiation during D-T operation. In the preliminary tritium experiment of JET (cf. REBUT et al. 1992) both a slight reduction of optical transmission as well as an enhanced fluorescence level was observed (MORGAN, 1992). Similar results were found at the TFTR tokamak (RAMSEY, 1992). If the fluoressence had a perflectly flat spectral distribution, any enhancement of the background would only act as an additional continuum level. The actual spectral distribution needs to be established in future experiments.
The fibre related fluorescence problems can in principle be avoided by a fibre-less optical link to remote instruments. Such a system has been recently been introduced at JET (cf. MORSI et al. 1991) and successfully tested during the preliminary tritium experiment. The system has, however, compared to a fibre optical link, a limitation in its maximum étendue due to the narrow optical labyrinth system which is needed for the reduction of neutron flux.

Summary and conclusions

We have attempted in this paper to give an overview of thermal and non-thermal alpha particle measurements at the JET tokamak for an energy range representative for helium beam fuelling experiments. The main effort was to establish a chain of quantitative consistency checks for the entire range between thermal energies up to the injection energy of 150 keV. The results have demonstrated clearly that in the first case, characterised by 'perpendicular view' , the observed fast particle spectra are compatible with the modelled charge exchange spectra based on anisotropic analytical Fokker Planck solutions for neutral beam injection. The second case, 'parallel' to the

toroidal field, is more complex, since the two spectral features representing non-thermal and thermal populations do overlap significantly and cannot be treated independently. This implies that either a time dependent analytical function comprising both features or a numerical treatment is required. This is especially the case for the initial fuelling phase where both populations are comparable in their respective densities. At the end of the fuelling phase, where a dominant Maxwellian and a true 'temperature' can be defined, the two separate analytic descriptions appear to be adequate.

Although the main emphasis of the present paper has been the presentation of the first observations at the JET tokamak of a fast ion population in the active charge exchange spectrum of HeII it appeared also essential to identify unambiguously the thermalised population. The reasons are manifold. The thermal population, its energy content and its density can be brought in immediate context with results of complementary diagnostic systems and its consistency may therefore be readily validated. The simultaneous observation of the two populations with comparable effective CX emssion rates and emission volumes enables a quantitative assessment of non-thermal particles, their density and their radial distribution. The helium fuelling experiments appear therefore to provide an ideal test-bed for alpha particle transport studies and the measurement of beam deposition and stationary helium ash profiles.

The JET results have also demonstrated that the complexity of the spectrum in the neighbourhood of the HeII 4686Å line does not present a principle problem for alpha particle diagnostics, and that the various contributing emission layers can be unambiguously identified and modelled. A more simple spectral structure is anticipated for the future pumped divertor phase of JET with a different toroidal viewing configuration leading to an effective red-shift of the slowing-down spectrum to the line free region on the red wing of the HeII line. The change-over of beryllium to graphite target plates in the divertor chamber will reduce in the case of the top-view configuration the contribution of the BeII and BeIV lines substantially.

And as a final remark, it should be pointed out that over the last years feasibility studies of CX based alpha particle diagnostics have varied in between quite optimistic to quite bleak outlooks for future fusion devices. The optimisation study presented in this paper has shown, that in the case of high target plasma densities (in excess of $n_e a = 10^{20} m^{-2}$), the lower stopping cross-sections of a neutral helium beam, and hence acceptable errors in the determination of beam densities, favourise strongly a neutral helium beam as a source for a quantitative diagnosis of alpha particles. This is inspite of lower CX emission rates compared to neutral hydrogen beam with the same energy per nucleon. For next-step fusion such devices such as ITER, with core densities of the order $10^{20} m^{-3}$ and line densities of $n_e a = 2 \cdot 10^{20} m^{-2}$, sensible signal-to-noise ratios

imply probe helium beam powers of 10 to 15 MWatt at 100keV/amu. This is still acceptable in view of the fact, that anticipated heating powers are of the order 500 MWatt. Progress in active helium beam emission spectroscopy may possibly reduce the constraints imposed by neutral beam attenuation calculations. The prospects for a resonable alpha particle diagnosis of the bulk of an ITER plasma appear therefore to be promising.

Acknowledgement

The consistency and validity checks of our results were supported by numerous critical and helpful discussions with many members of the JET team. The patience and efficiency of Mark Wallwork who rewrote and updated the CX spectral analysis program is also much appreciated.

References:

Anderson, D.J. J.Plasma Phys. (1983) **29**,317

Core W.G.F. , JET-IR(91)15

Boileau A., von Hellermann M., Horton L.D., Spence J., Summers H.P. (1989) Plasma Phys. Contr. Fusion **31**,779

Boileau A., von Hellermann M., Mandl W., Summers H.P., Weisen H., Zinoviev A. (1989) J.Phys.B At. Mol.Opt. Phys. **22**,L145

Danielsson M., von Hellermann M.G., Kallne E., Mandl W., Morsi H., Summers H.P., Zastrow K.D ,Rev.Sci.Instr.(1992),**63**, 2241

Fonck R.J, Darrow D.S., Jaehnig et al., Phys.Rev. (1984) **29**,3288

Frieling J., PhD thesis, University of Amsterdam 1993

Holmes A.,(1992) Plasma Phys.Contr.Fus. , **34**,653

Howell R.B., Fonck R.J., Knize R.T., Jaehnig K.P. (1988) Rev.Sci.Instr.**59**,1521

Kolesnichenko, Ya. I., Yakovenko Yu. V., (1992), Nuclear Fusion,**32**,449

Mandl W., PhD Thesis, University of Munich, 1991, JET-IR(92)05

Mandl W., Wolf R.C., von Hellermann M., Summers H.P., submitted to Plasma Physics and Contr. Fusion 1992

Marcus F. et al. (1992), Plasma Phys. Contr. Fus.,**34**, 1371

Morgan P.D. 7'th Symposium on Fusion Technology, Rome, Italy, 1992, JET-P(..)92

Morsi H. , Hatzky R., von Hellermann M., Mandl W., McKillen R., Mijnarends M., Millward P., Nielsen P., Reid J., Roberts P., Ryan J., Thomas P., Viaccoz B. (1991) Proc. EPS 1991, Berlin

Mukhovatov V. et al. ITER diagnostics (1990), IAEA Vienna

Post D.G., 'International Workshop on Helium Transport and Exhaust' (1991) Nuclear Fusion, **31**,2181, Editor J.Hogan, D.Hillis

Ramsey A., K.W.Hill, (1992) Rev.Sci.Instr. **63**, 4735

Rebut P.H. and the JET team (1992) Nuclear Fusion, **32**, 187

Summers H.P., von Hellermann M., Breger P., Frieling J., Horton L.D., Koenig R., Mandl W., Morsi H., Wolf R., de Heer F., Hoekstra R., Fritsch W. (1992) Proc., 'Atomic Processes in Plasmas'

Summers H.P., Dickson W., Boileau A., Burke B.G., Denne-Hinnov B., Fritsch W., Giannella R., Hawkes N.C., von Hellermann M., Mandl W., Peacock N.J., Reid R., Stamp M.F., Thomas P.R. (1991) Plasma Phys.Contr.Fusion **34**,325

Synakowski E.J., Stratton B.C., Efthimion P.C., Fonck R.J., Hulse R. , Johnson D.W., Mansfield K., Park H., Scott S.D., Taylor G. (1990) Phys. Rev.Lett. **65**,2255

von Hellermann M., Mandl W., Summers H.P., Boileau A., Hoekstra R., de Heer F., Frieling J. (1991) Plasma Phys.Contr.Fusion, **33**,1805

von Hellermann M., Mandl W., Summers H.P., Weisen H., Boileau A., Morgan P.D., Morsi H., Koenig R.T.W., Stamp M.F., Wolf R.C., (1991) Rev. Sci. Instr. **61**,3479

von Hellermann M. and Summers H.P. (1992), Rev. Sci. Instr. **63**, 5132

Weisen H., von Hellermann M., Boileau A., Horton L.D., Mandl W., Summers H.P. (1989) Nuclear Fusion, **29**, 2187

Weisen H., Bergsaker H., Campbell D.J., Erents S.K. , de Kock L.C., McCracken G.M., Stamp M.F., Summers D.R., Thomas P.R., von Hellermann M., Zhu. J. (1991) Nuclear Fusion, **31**, 2247

Wolle B., Eriksson L-G (1992), JET-P(92)30, submitted to Plasma Phys. Contr. Fusion

Young K.F., Proc. ICPP 1992, Innsbruck

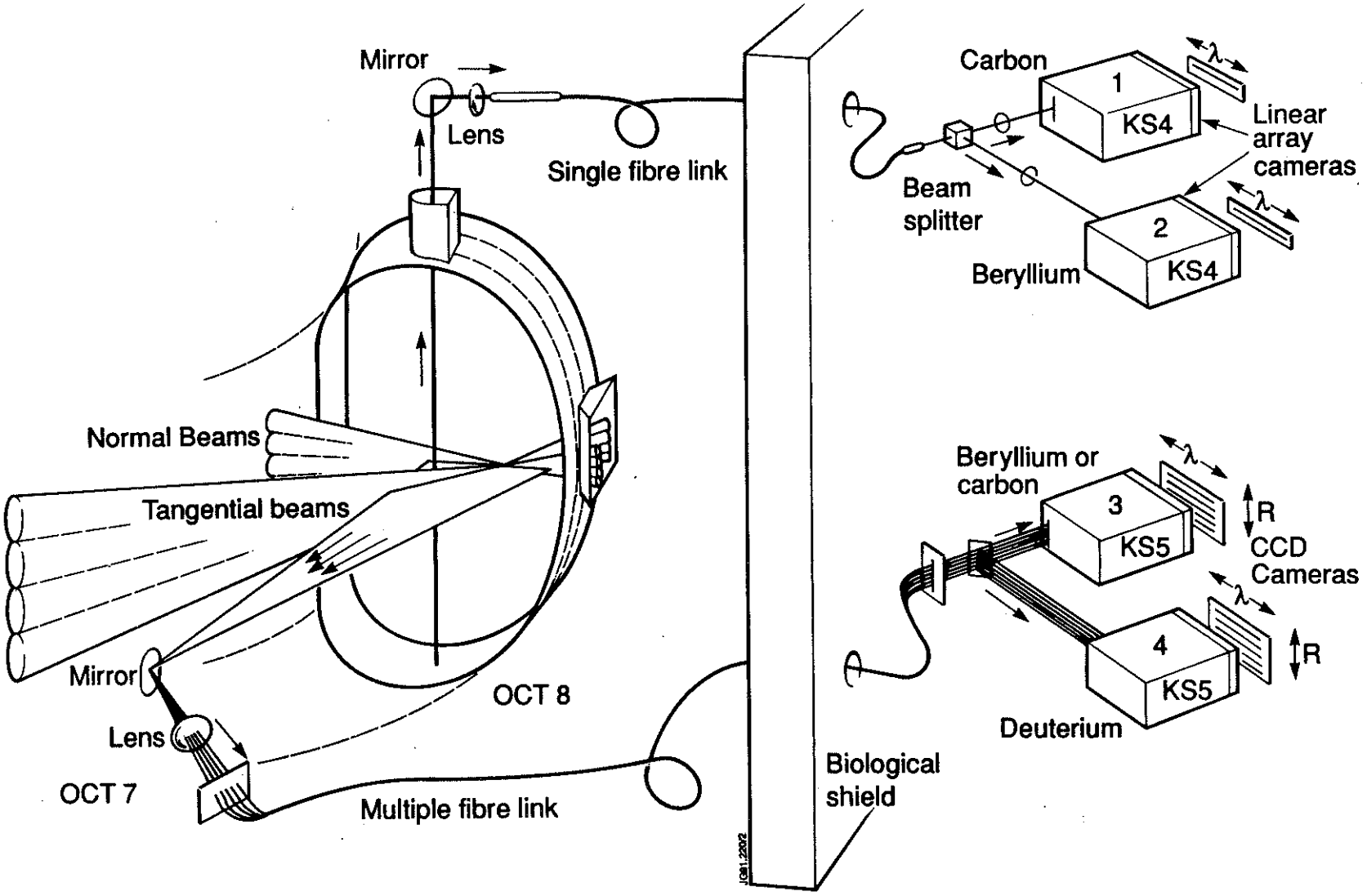

Fig.1 Layout of the JET CXRS diagnostic and its instrumentation

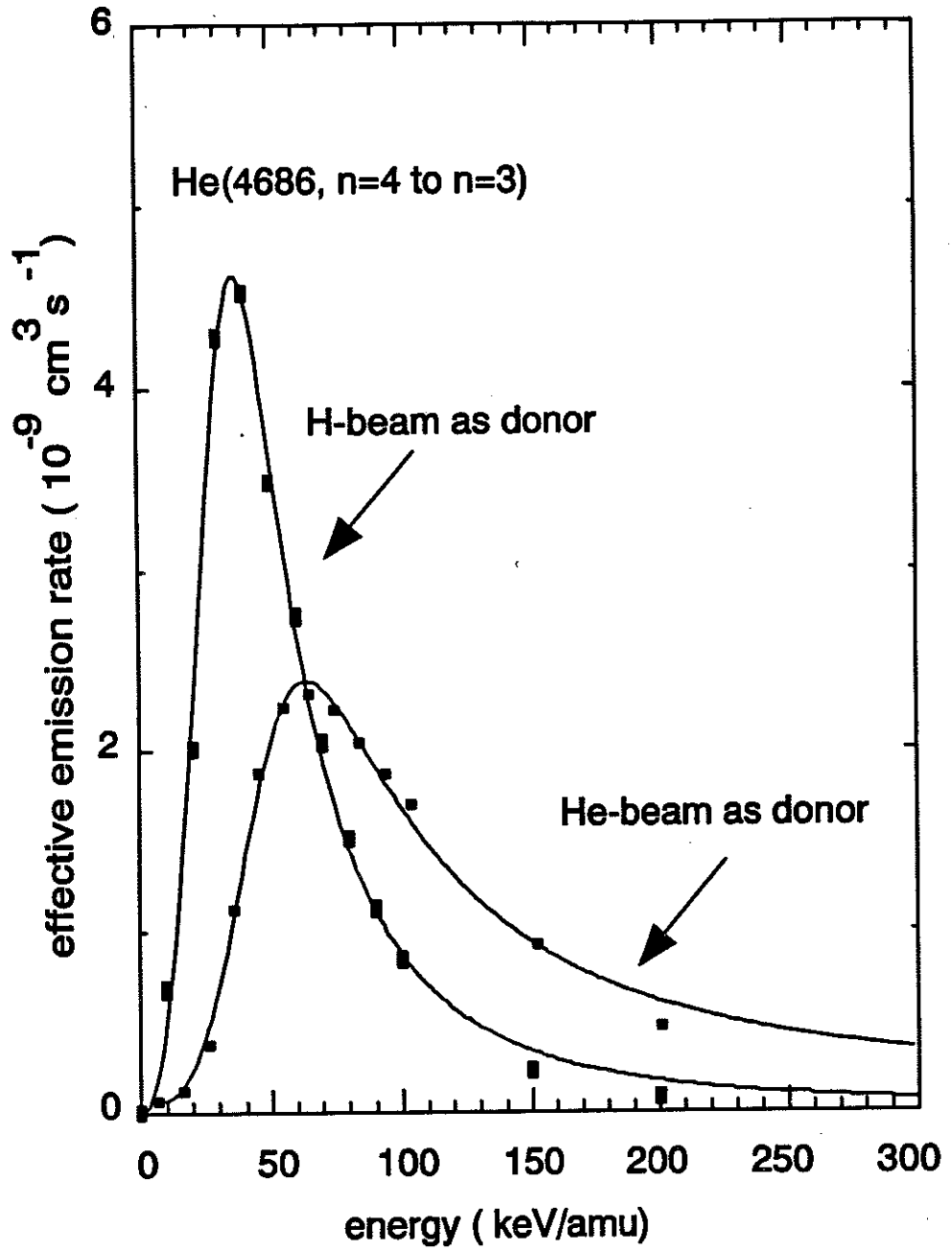

Fig.2 Effective emission rates for the He (n=4-3, λ=4686Å) transition for **a**) a hydrogen neutral beam and **b**) a helium neutral beam as an electron donor. The effective rates are calculated for standard values of $n_e=3\cdot10^{19}m^{-3}$, $T_e=T_i=$ 10keV, and $Z_{eff}=$ 2. A parametric fit to cross-section values at a set of discrete energies is used for the calculation of observed thermal and slowing-down spectra.

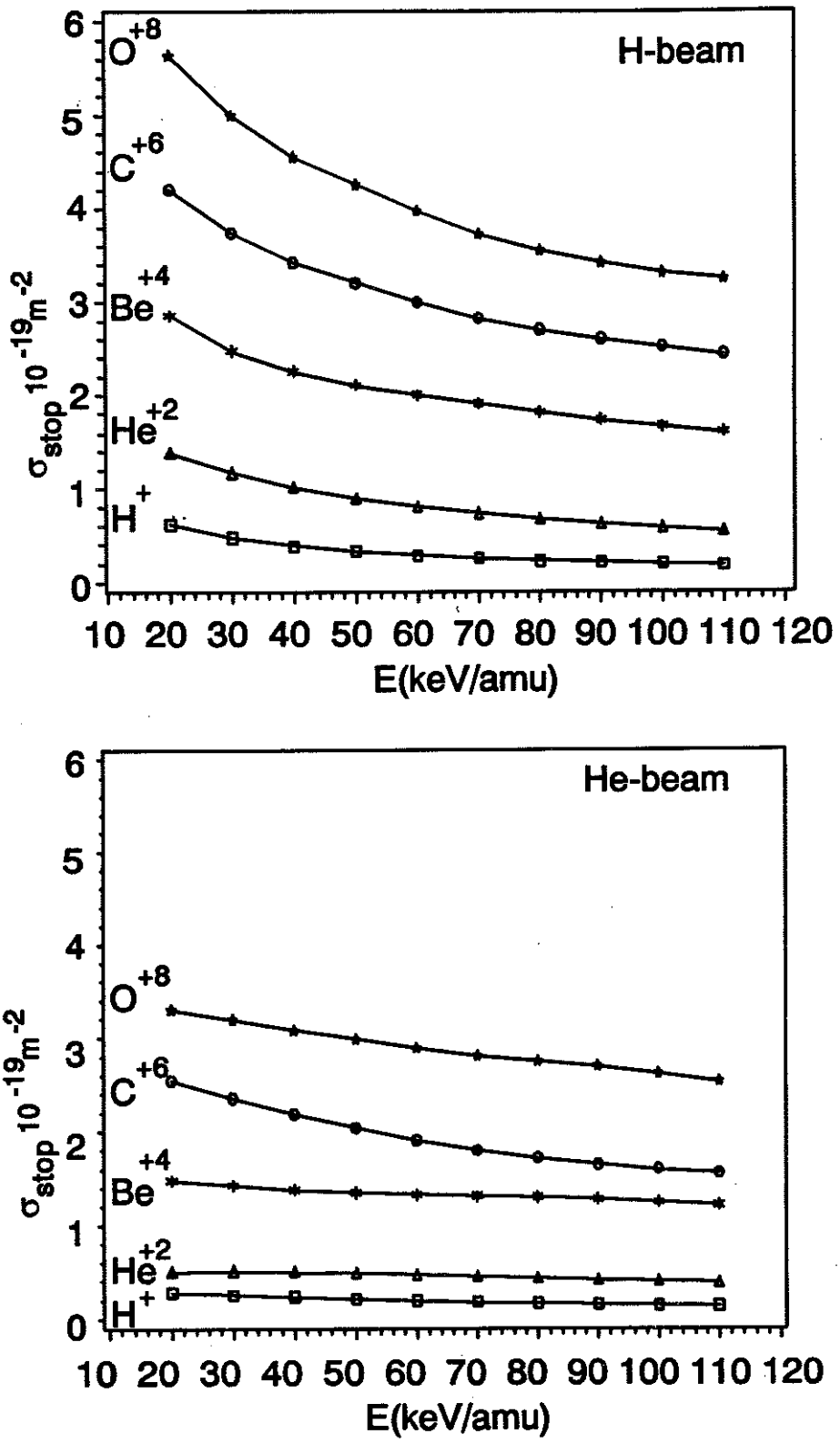

Fig.3 Total stopping cross-sections for **a)** H and **b)** He neutral beams interacting with the main light impurities in a plasma. The total cross-section refers to the sum of electron and ion ionisation and charge exchange intractions. The cross-sections are calculated for a moderate electron density of $3 \cdot 10^{19} m^{-3}$, where multiple step processes are neglible.

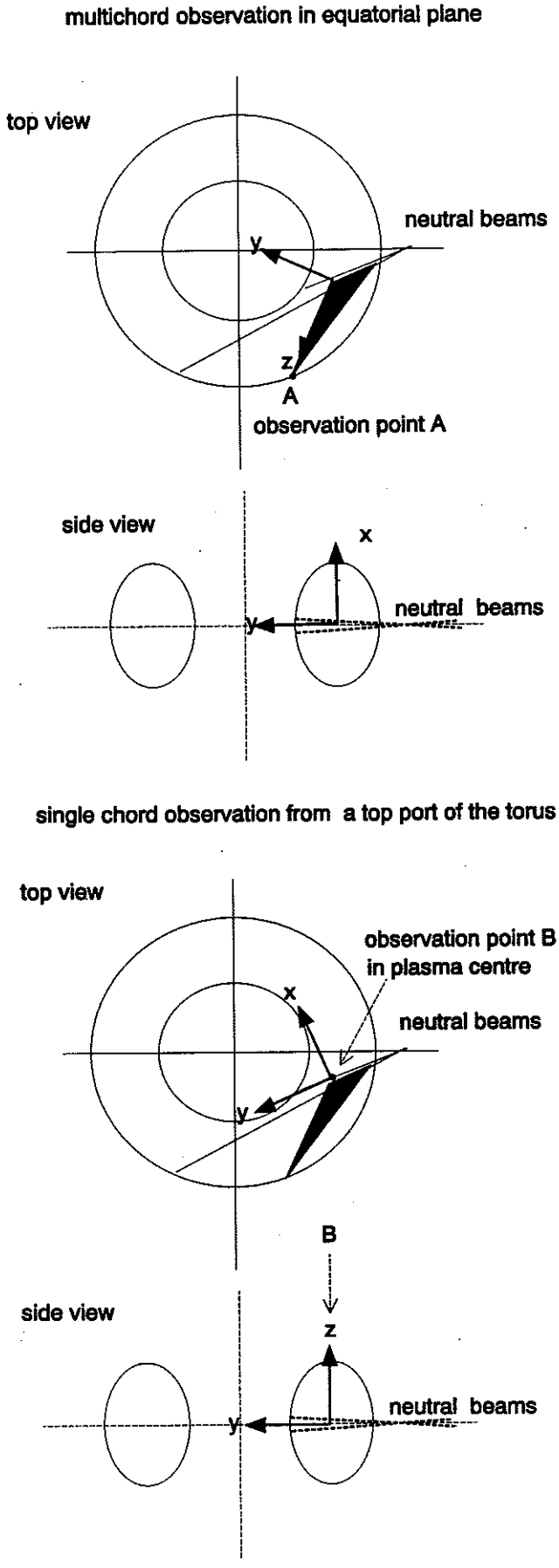

Fig.4 a) 'perpendicular' viewing geometry using a top port of the torus **b)** 'parallel' viewing geometry with an observation port close to the equatorial midplane of the JET torus, showing the orientation of the respective viewing co-ordinate systems.

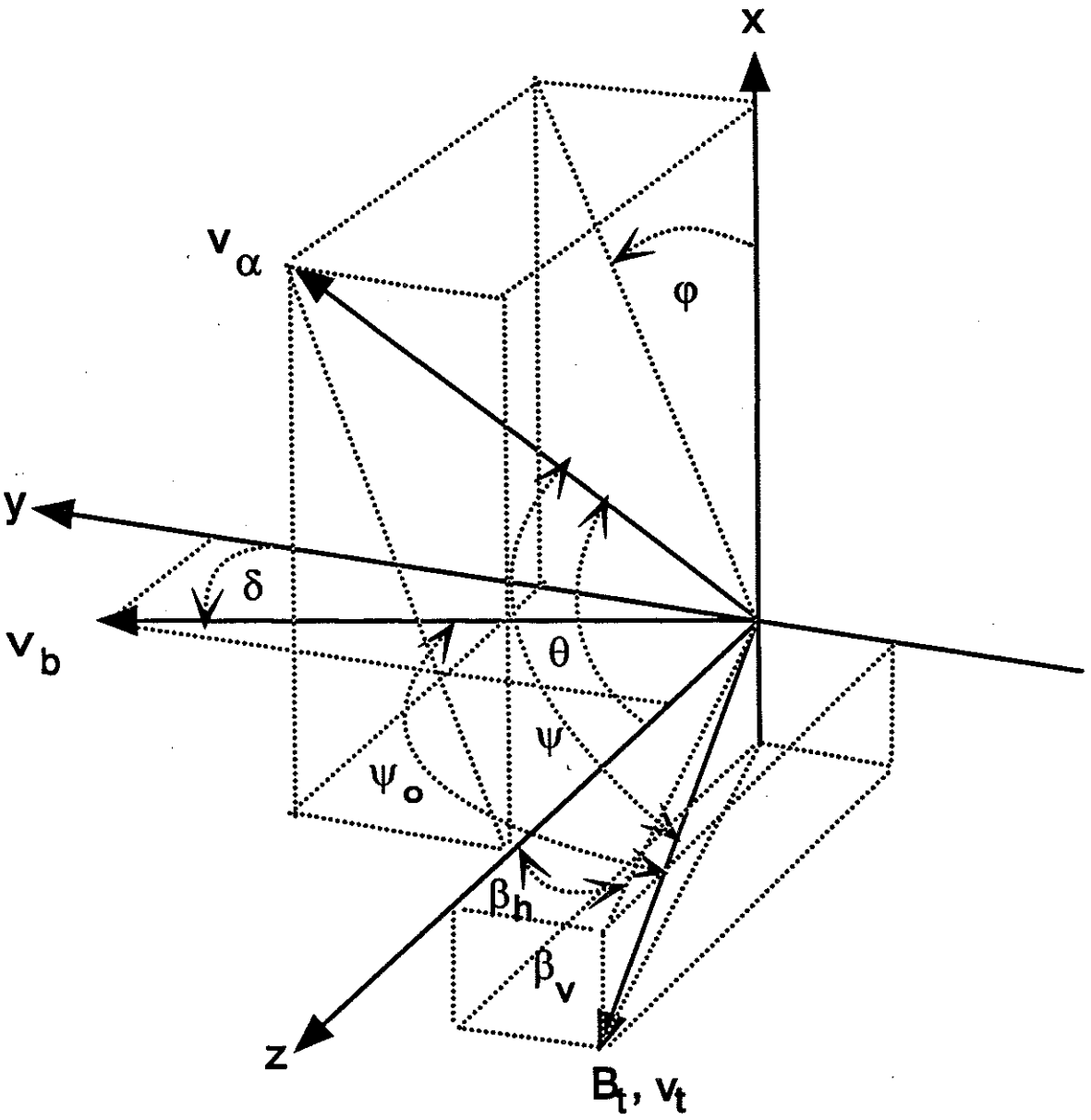

Fig.5 Viewing co-ordinate system and relevant angles: z-axis in viewing direction, velocity vector v_b of neutral beam in y-z-plane, ψ_0 angle between neutral beam and magnetic field, ψ angle between alpha particle and magnetic field, δ angle between neutral beam and y-axis, angles β_h and β_v define the orientation of the toroidal magnetic field.

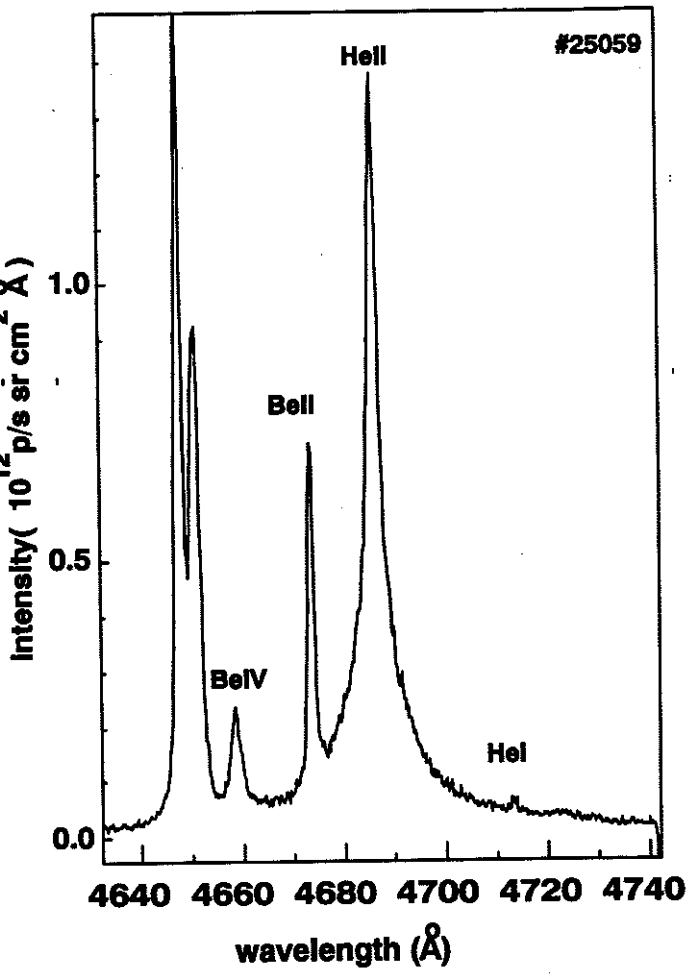
#25059
HeII
BeII
BeIV
HeI
1.0
0.5
0.0
Intensity(10^{12} p/s sr cm^2 Å)
4640 4660 4680 4700 4720 4740
wavelength (Å)

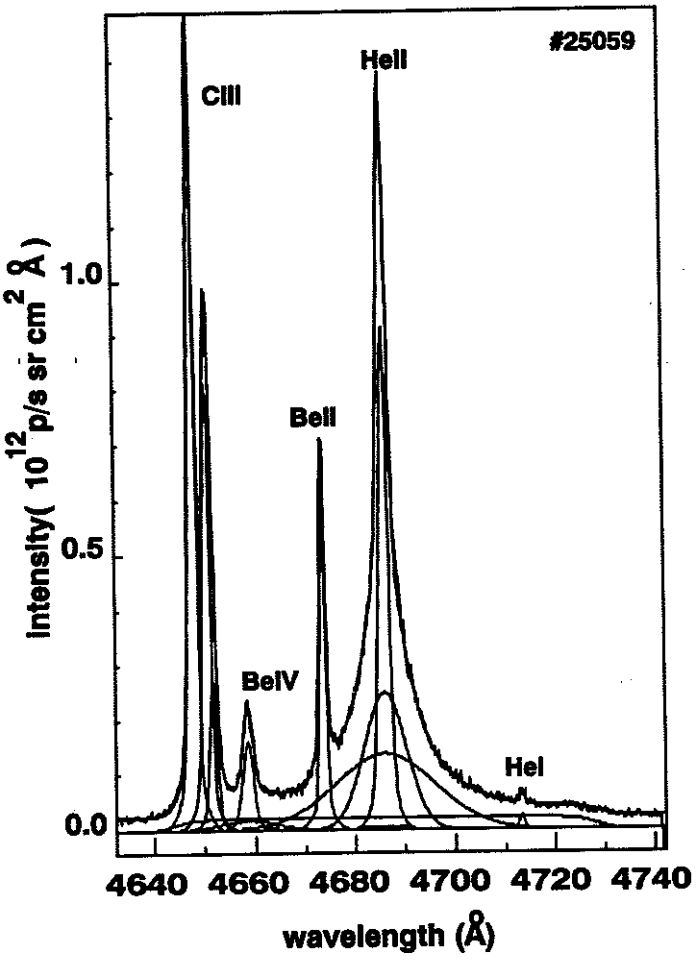
#25059
CIII
HeII
BeII
BeIV
HeI
1.0
0.5
0.0
Intensity(10^{12} p/s sr cm^2 Å)
4640 4660 4680 4700 4720 4740
wavelength (Å)

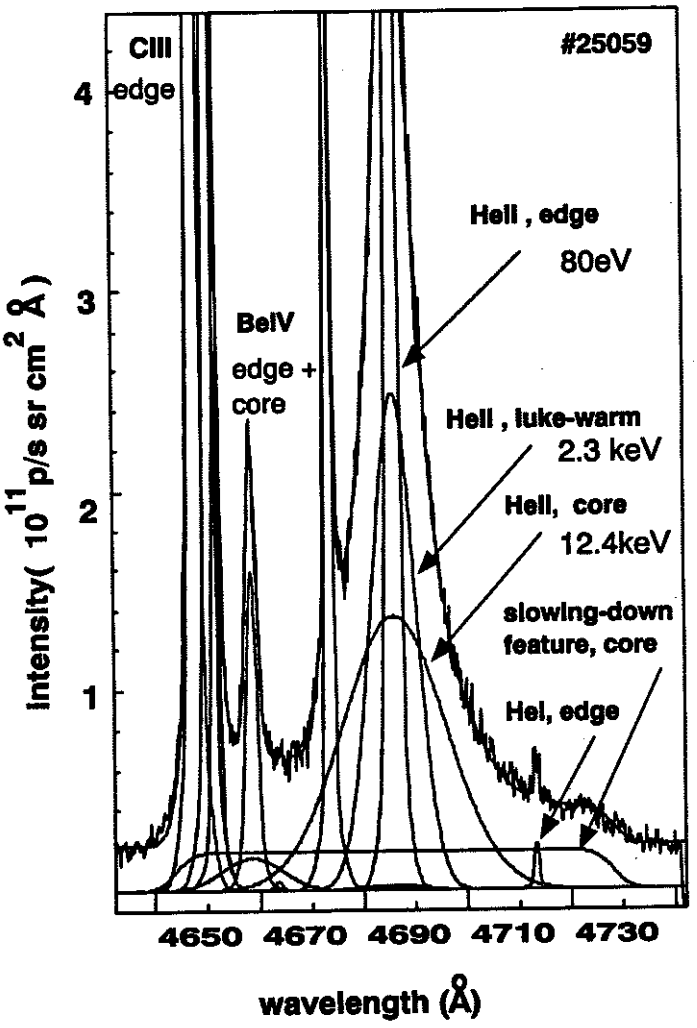

Fig.6 Thermal and non-thermal features in the He-Be spectrum ('top-view'), a) overview, b) fitted components, c) enlarged section showing the broad band slowing-down pedestal.

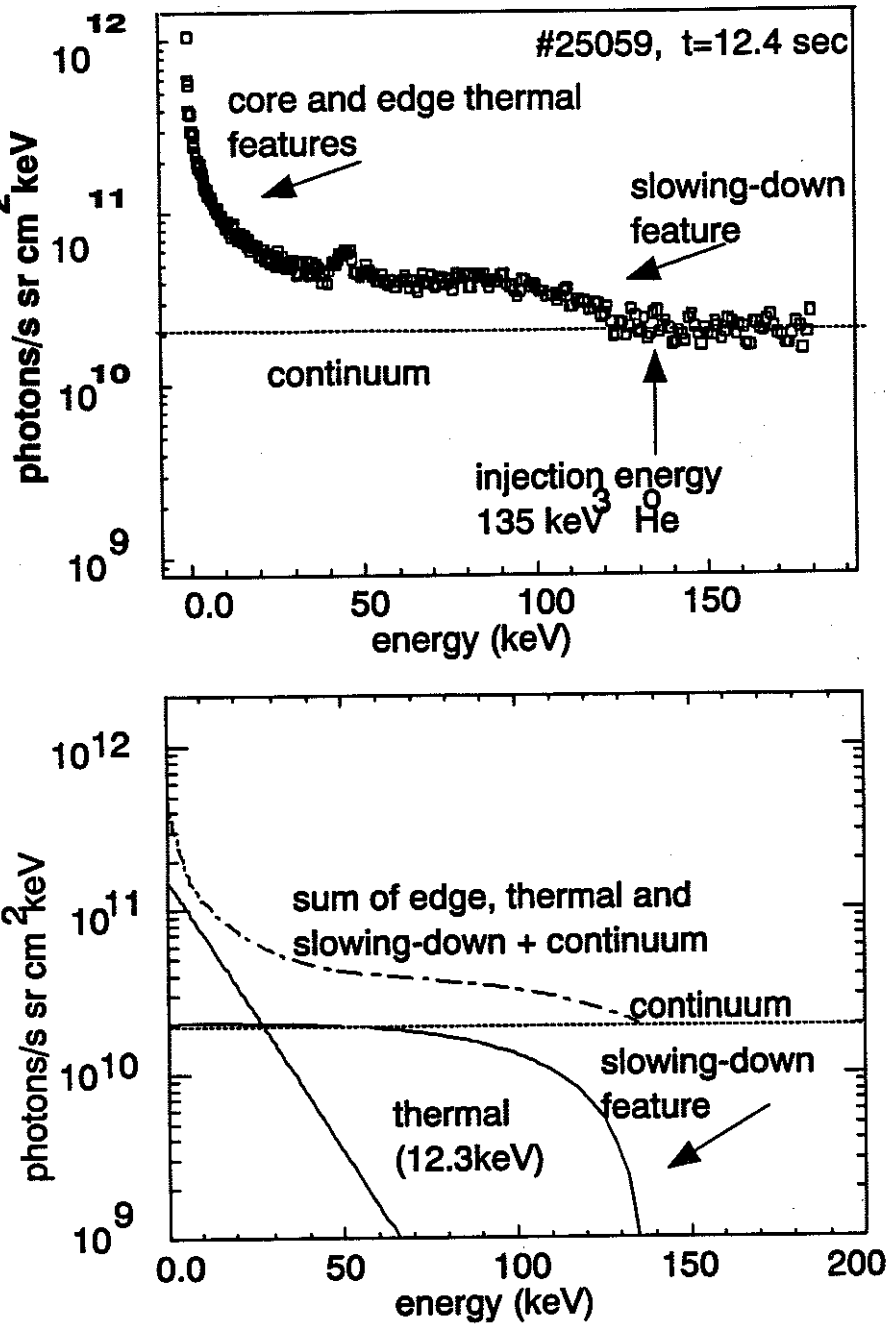

Fig.7 Logarithmic presentation of 'top-view' spectrum with intensity versus energy, **a)** experimental, **b)** simulation based on anisotropic slowing-down function

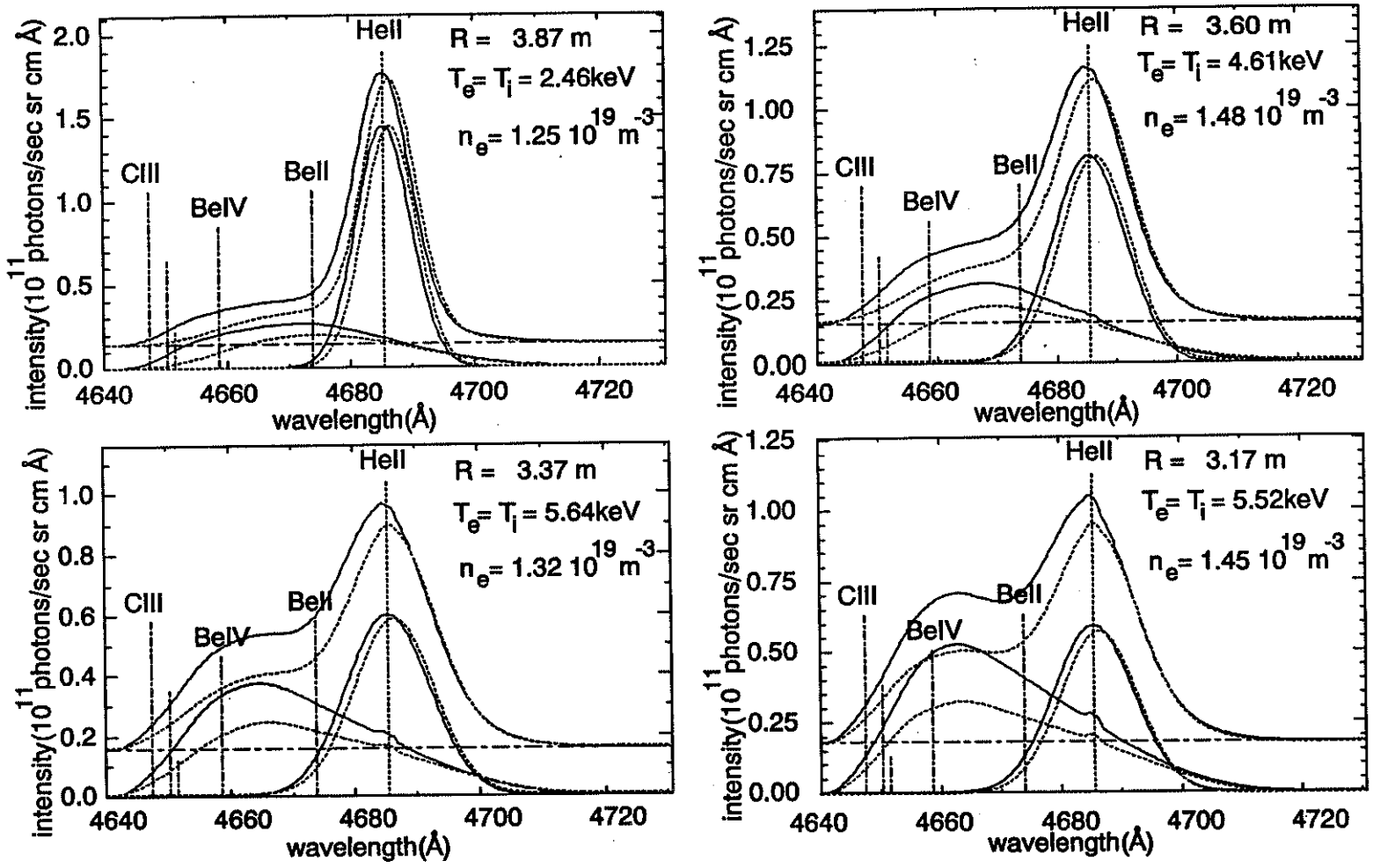

Fig.8 Simulated spectra for 4 radial positions, **a)** solid lines, calculated for the case of constant emission rate $Q_{cx}(E_{coll}=E_{beam})$, and **b)** dashed lines, for the actual case of varying emission rates $Q_{cx}(E_{coll}=f(v_{alpha}, v_{beam}))$. The spectral shapes of thermal and non-thermal populations are basically sustained, but with reduced amplitude width and apparent Doppler shift.

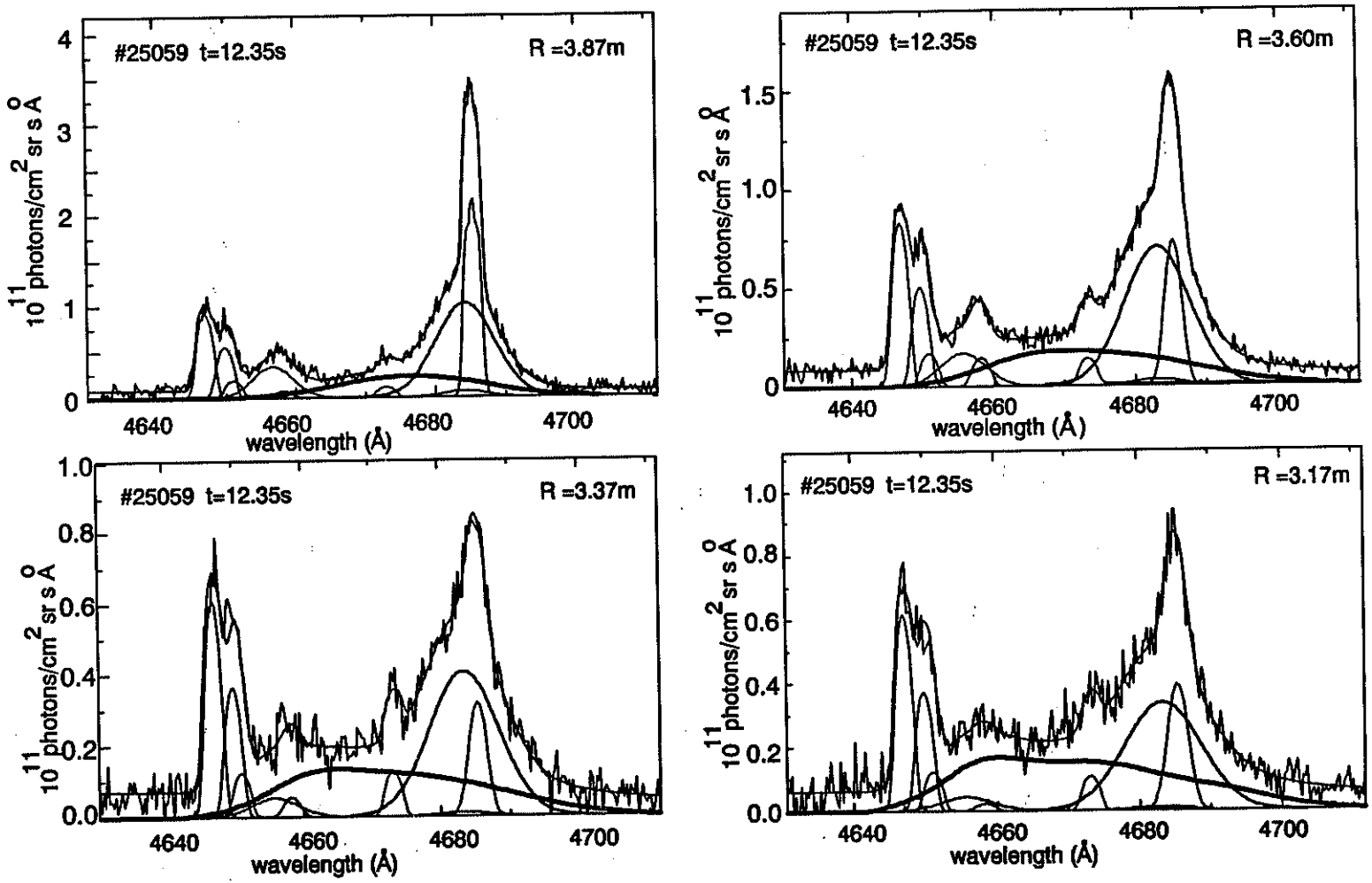

Fig.9 Experimental spectra for the same radial points showing the passive background spectra of HeII, BeII and BeIV , and the Doppler shifted thermal CX spectra of HeII and BeIV and the anisotropic non-thermal slowing-down spectrum. Two representative time slices are shown, one at the beginning of the fuelling process **a)**, and **b)** the same spectra at a later time when the thermal population dominates. Note also that the ratio of BeIV to HeII changes over the radius illustrating the effects of central fuelling.

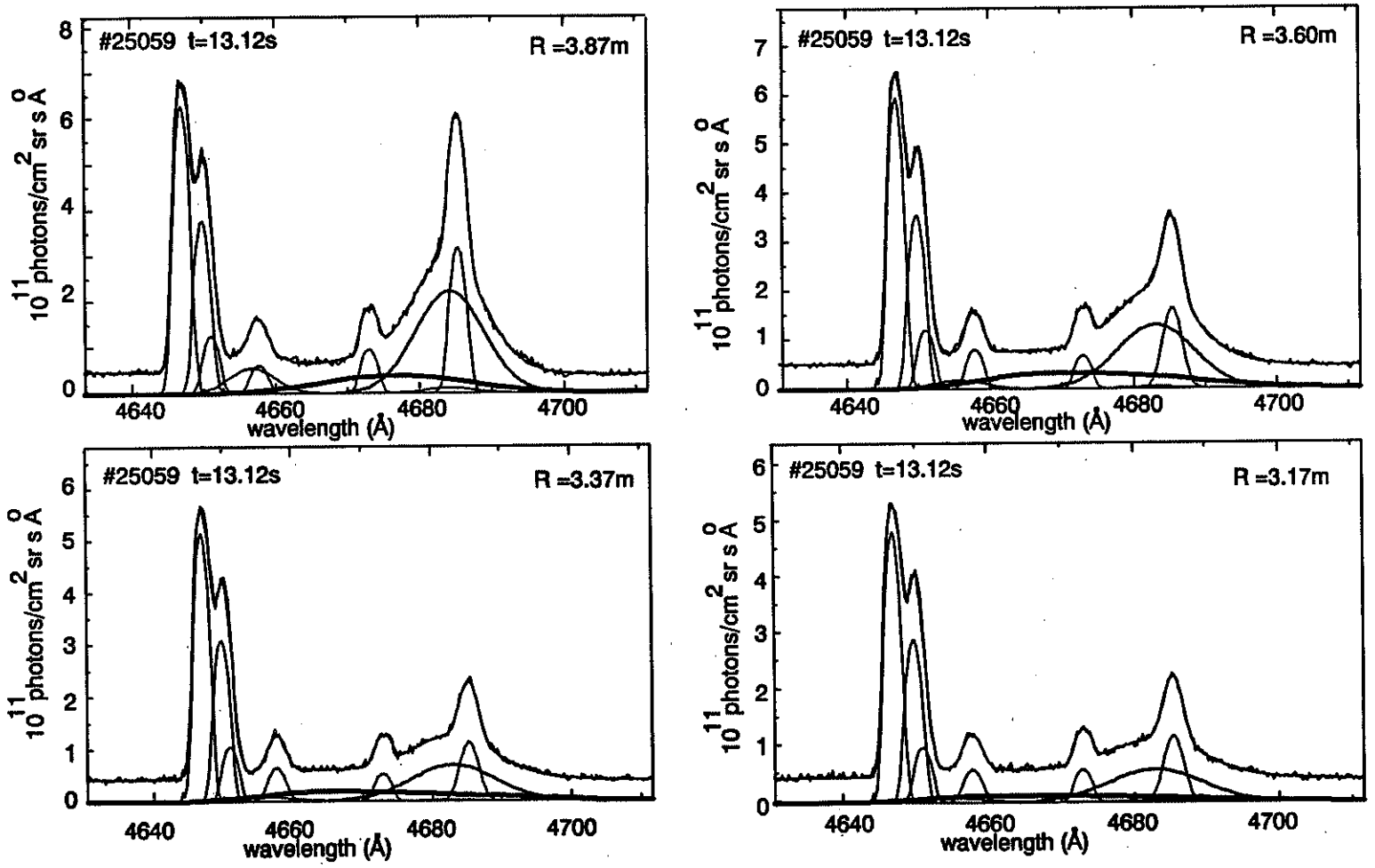
#25059 t=13.12s
R =3.87m
#25059 t=13.12s
R =3.60m
#25059 t=13.12s
R =3.37m
#25059 t=13.12s
R =3.17m
10^11 photons/cm^2 sr s Å
wavelength (Å)
4640
4660
4680
4700

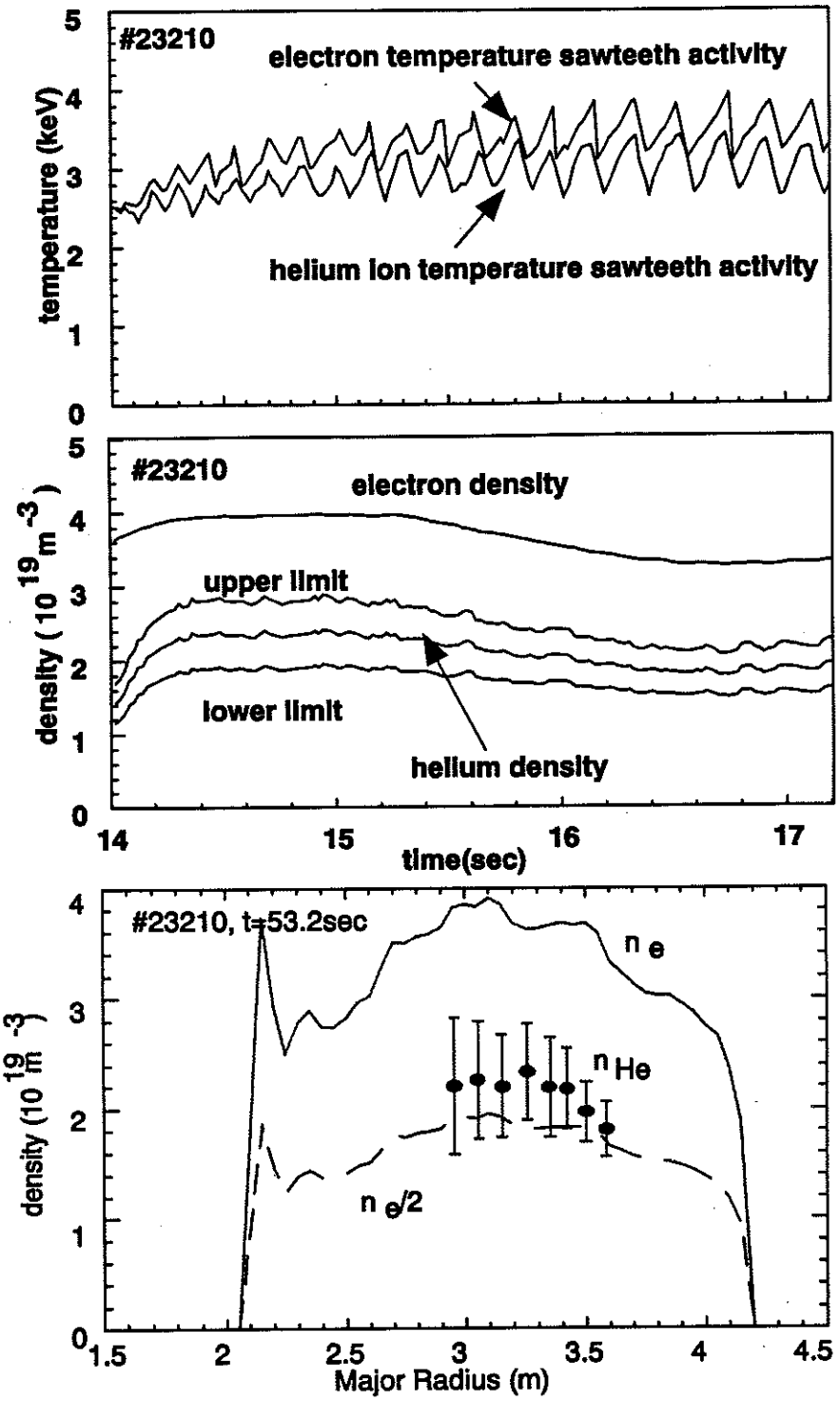

Fig.10 a)Ion and electron temperatures in sawteething low-temperature pure helium discharge (#23210), b) electron density (FIR interferometer) and helium density (CXRS), c) radial density profiles of electrons (LIDAR) and thermal alpha particles deduced from CXRS measurements .

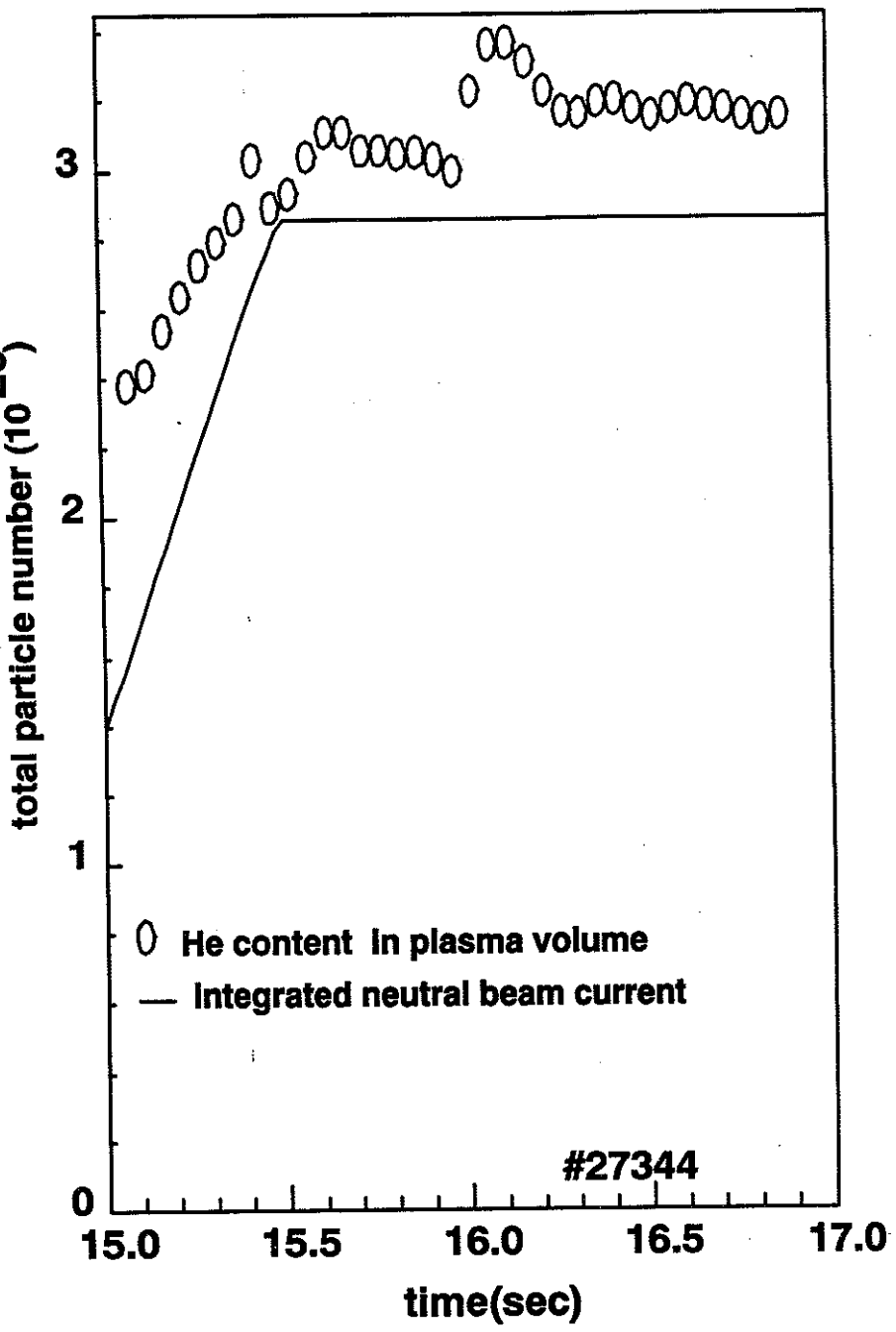

Fig.11 Neutral beam current and total plasma helium content derived from the volume integrated thermal helium density profile (pulse #27344).

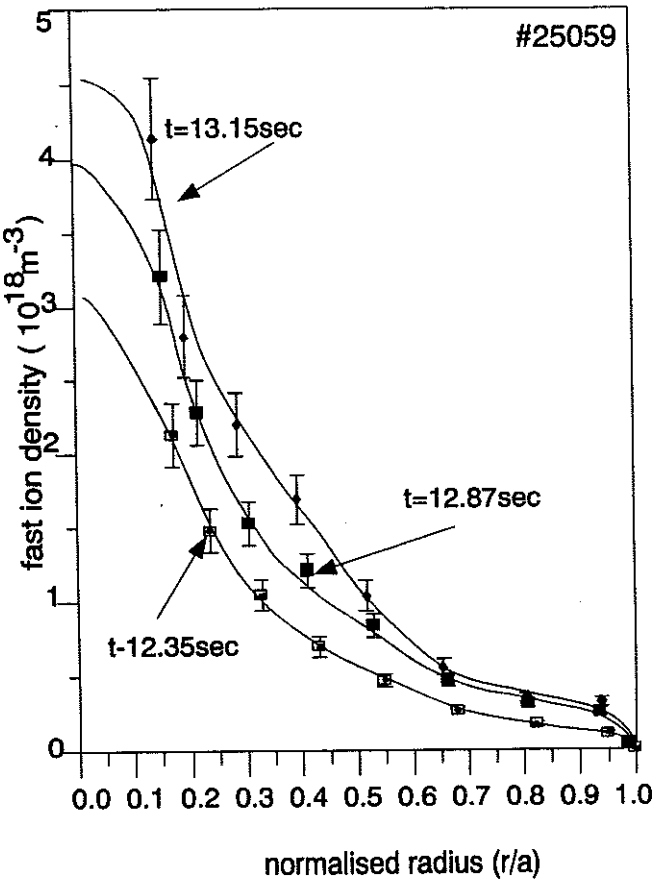

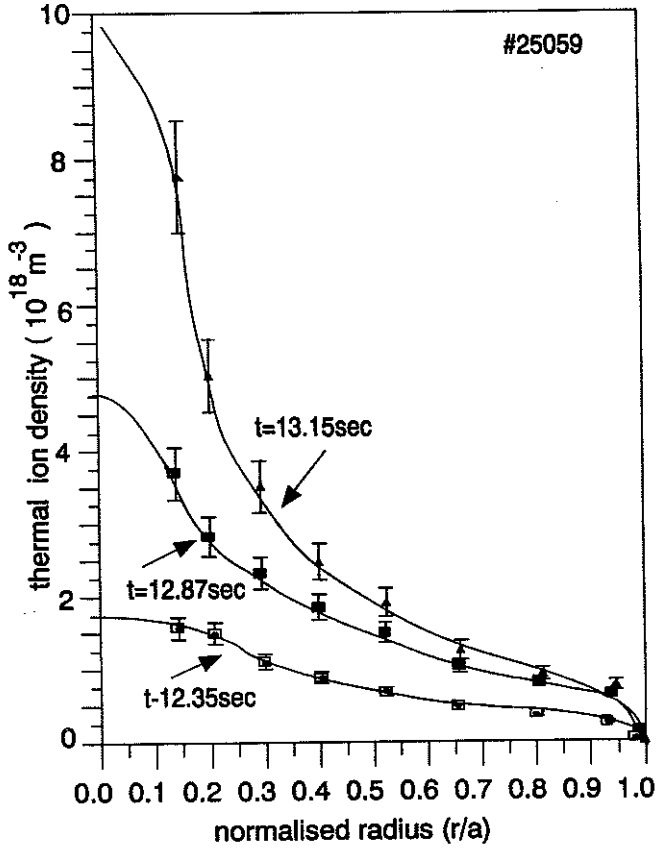

Fig.12 Radial profiles of a) fast and b) thermal alpha particle densities in a high-power, low-density helium beam heated JET plasma. The time slices are indicated in the overview of Fig. 13 .

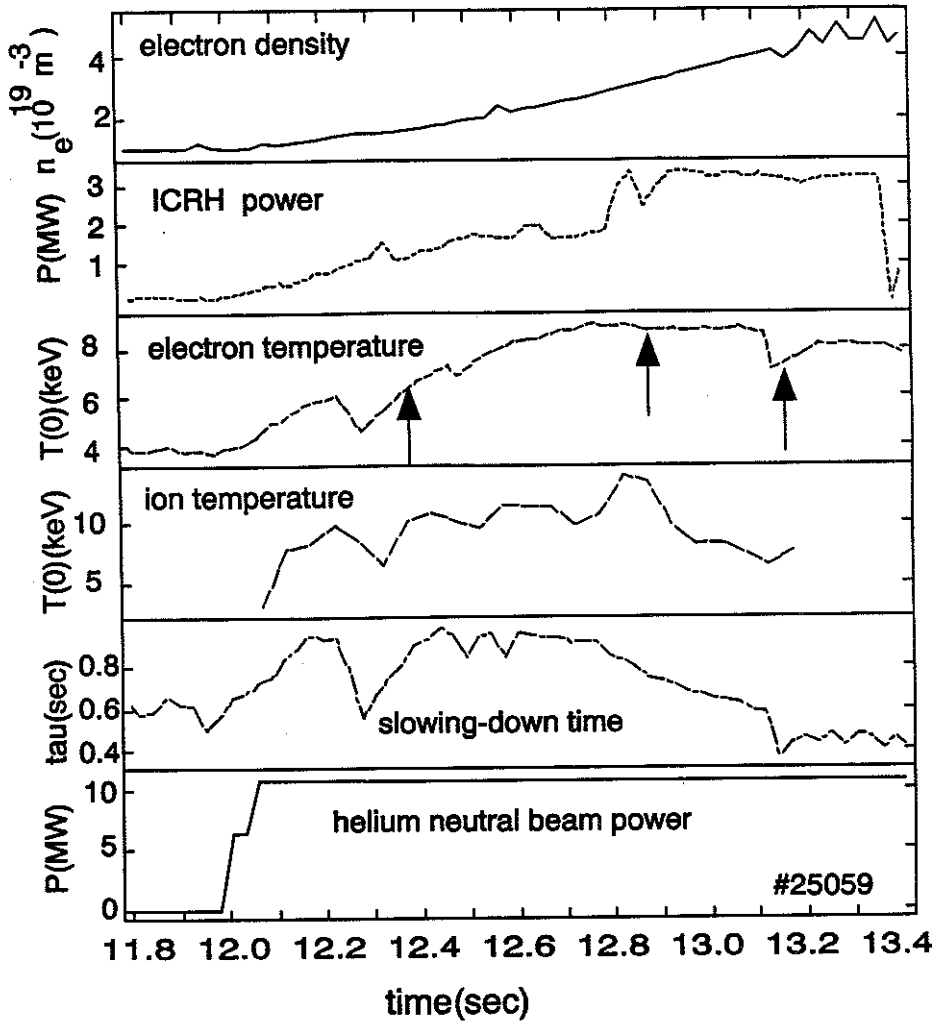

Fig.13 Survey of main plasma data in a hot-ion mode, helium beam heated deuterium plasma (pulse #25059), **a)** heating powers P_{NBI} and P_{RF}, **b)** temperatures T_e, T_i, **c)** electron density n_e, and impurity density n_{He} **d)** alpha particle slowing-down time τ_s.

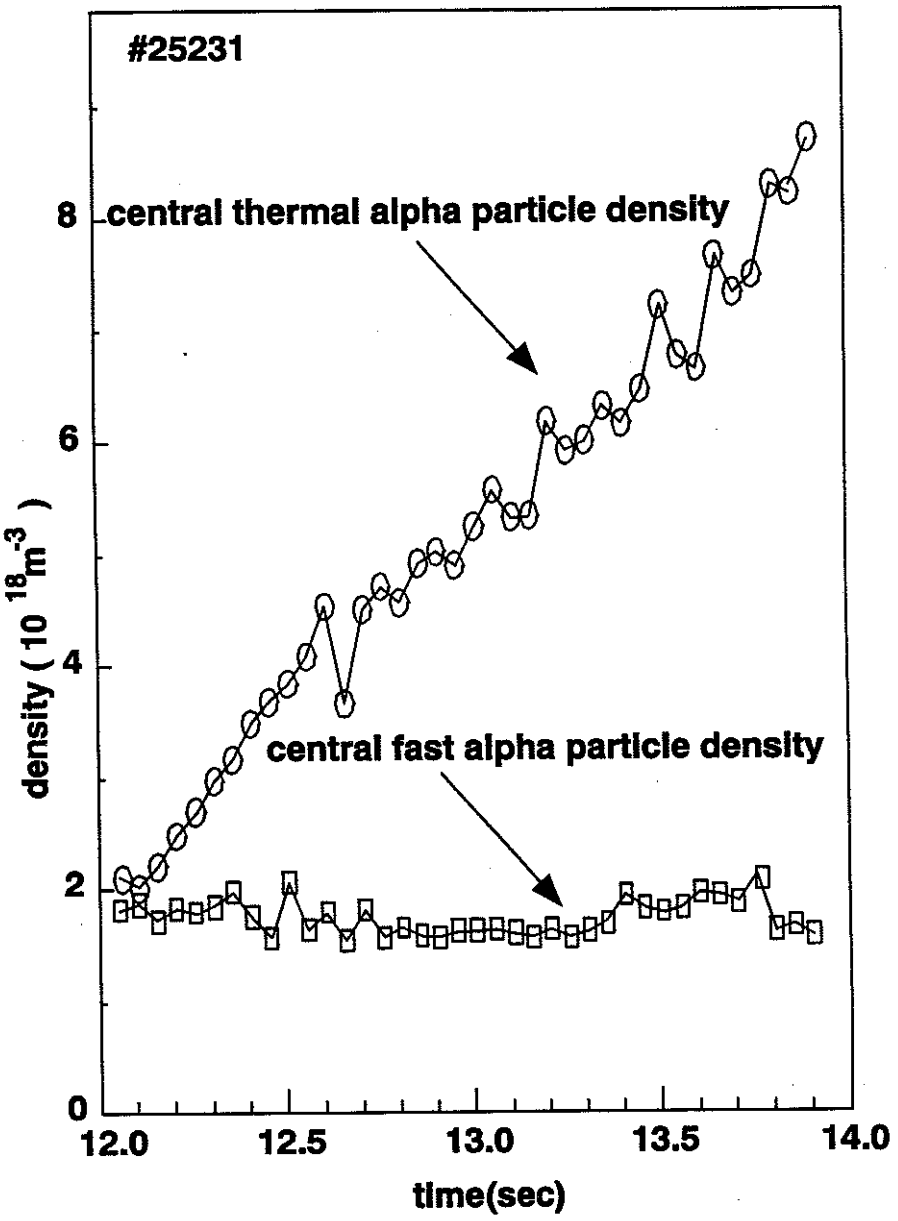

Fig.14 Thermal and non-thermal helium ion densities in the course of a helium fuelling pulse (pulse #25231)

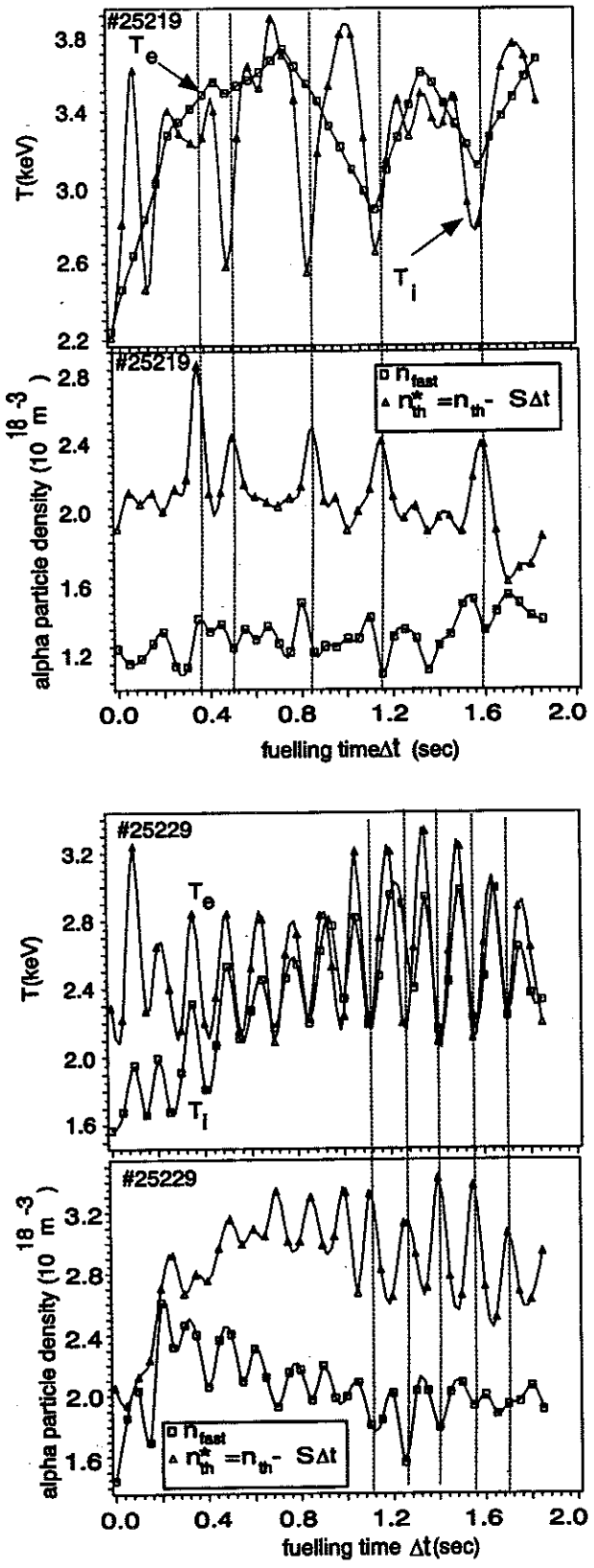

Fig.15 Sawteeth oscillation of fast and thermal ion densities in a low-power NB heating pulse with no additional RF heating. In order to compare both oscillations the linear rise in the thermal density is removed by plotting the 'reduced' thermal density $n^* = n_{th} - S \cdot \Delta t$, where Δt is the fuelling time and S the fuelling rate. Two cases are shown with a relatively short sawtooth period **a)** and a slightly longer one **b)** showing the phase delay between fast and thermal helium density.

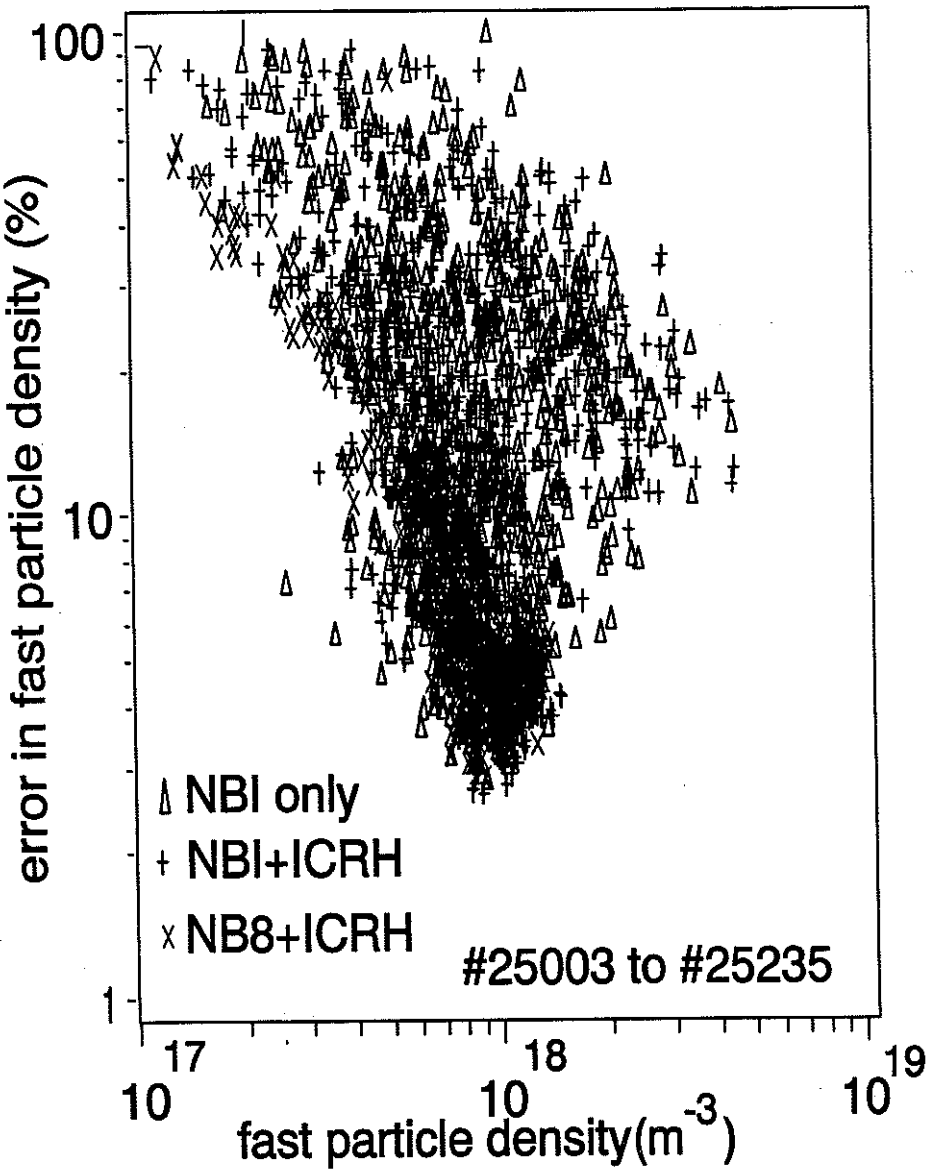

Fig.16 Overview of fast central ion densities detected in the JET helium heating and their respective statistical error bars.

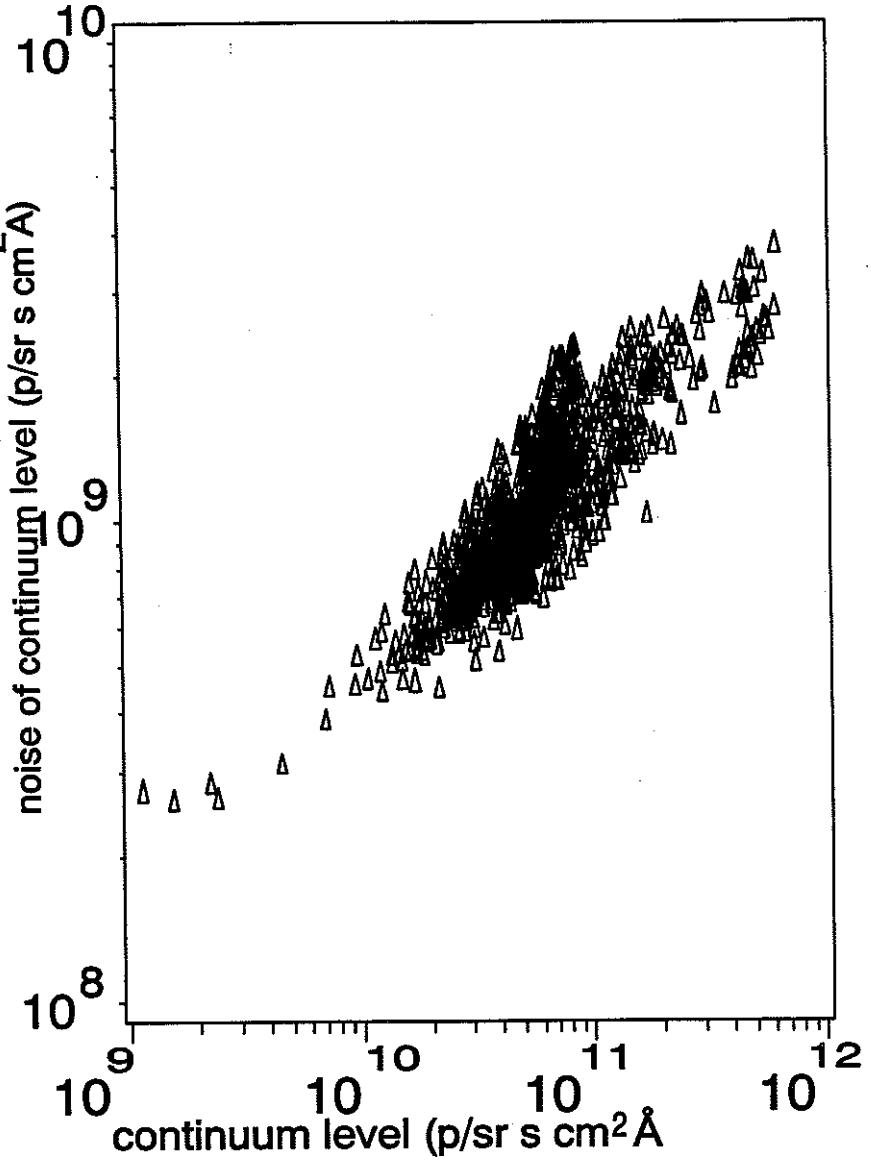

Fig.17 Bremsstrahlung levels and rms noise showing the Poisson square root characteristics observed over several orders of magnitude.

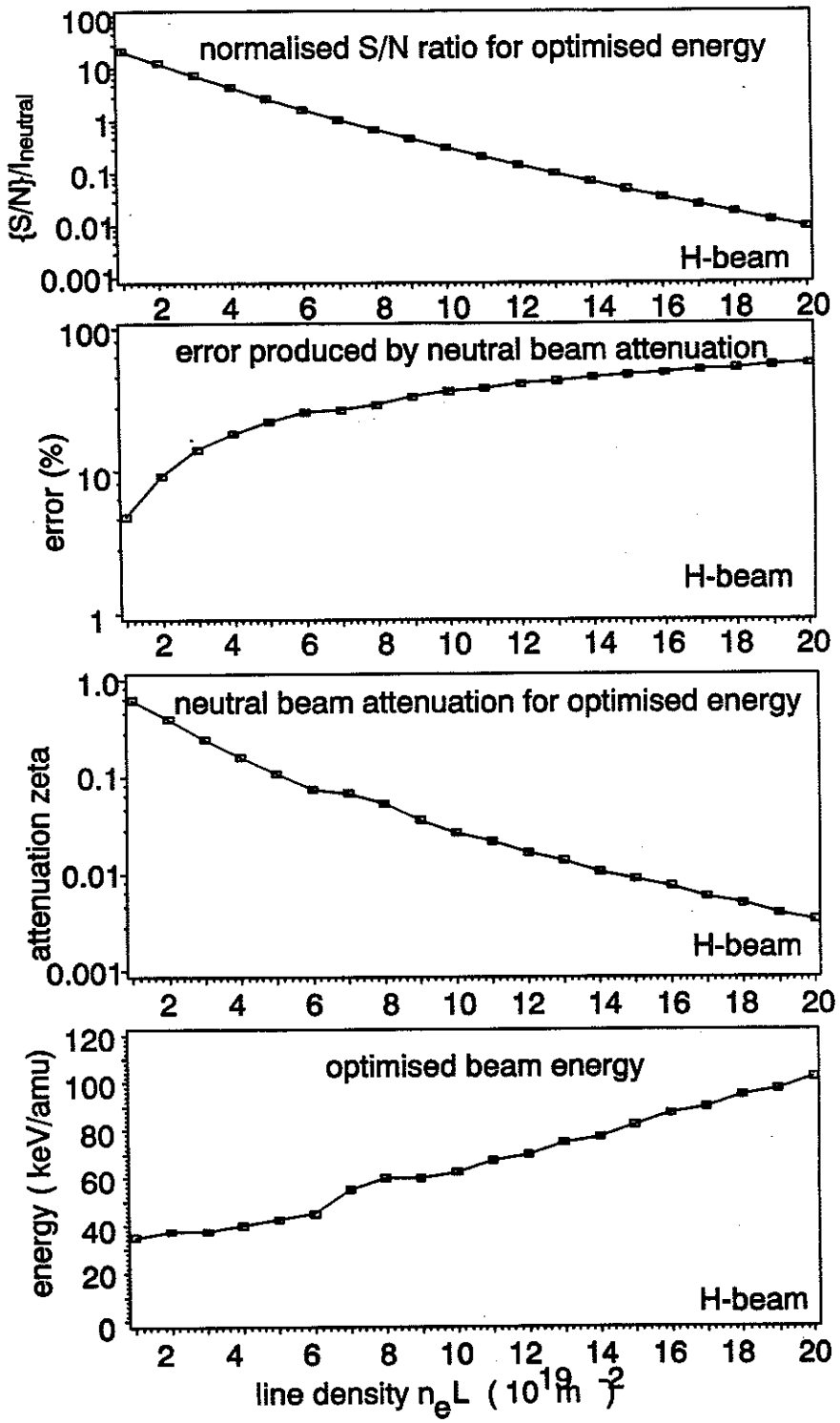

Fig.18 a) Normalised signal-to-noise ratio $\{S/N\}/I_n$ versus line integrated density for the case of a 5% alpha particle concentration and a hydrogenic (Z=1) probe beam. Note that the beam energy is optimised for each density density value reflecting the trade-off between beam attenuation and emission rates **b)** error propagation produced by the exponential attenuation process, **c)** attenuation factor, **d)** optimised energy.

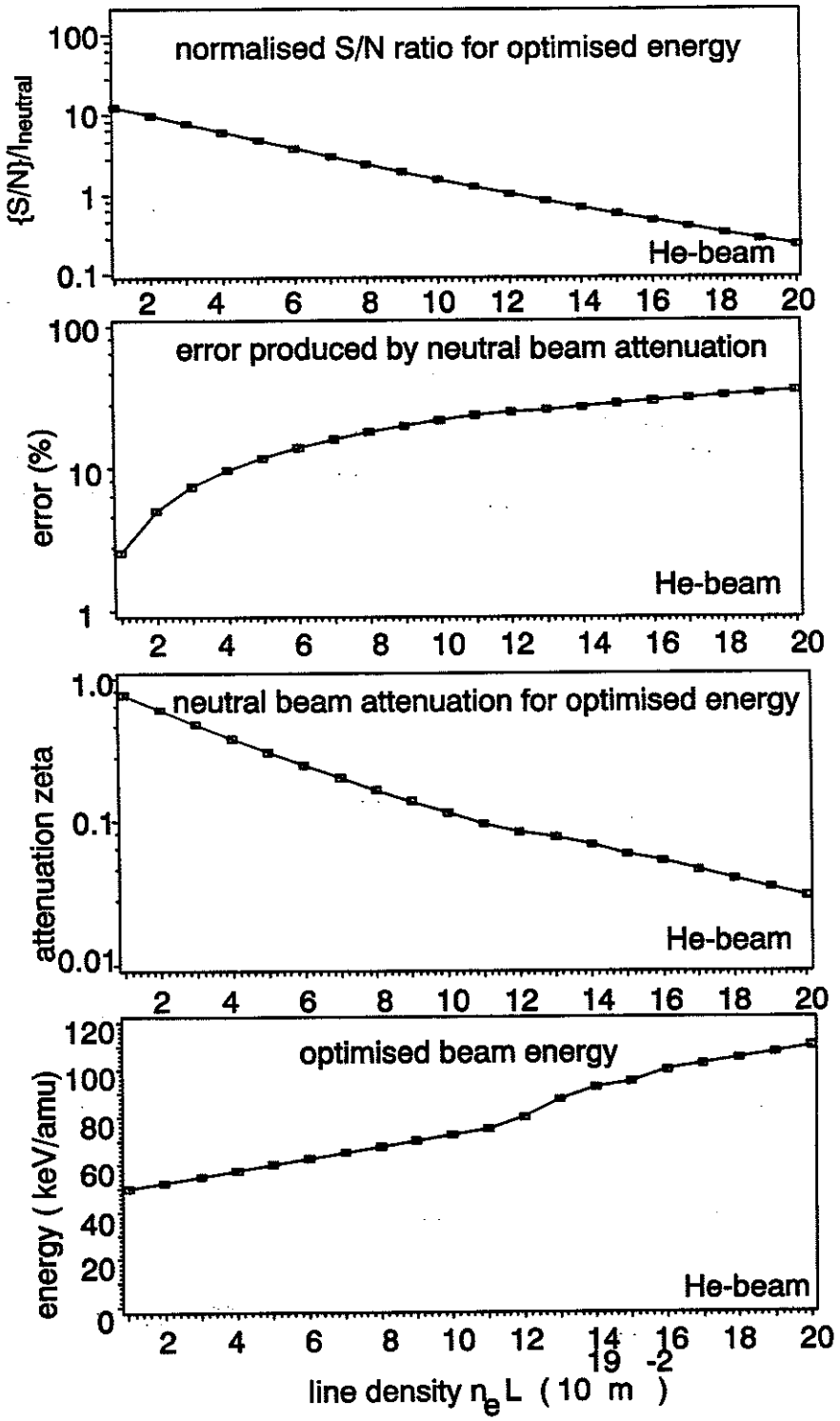

Fig. 19 The same data for a neutral helium beam. The lower stopping cross-sections lead to a significantly reduced error in the beam attenuation and also to considerably higher values of S/N, which may be reached at high densities. The optimum S/N values are however achieved at the cost of appreciable higher neutral beam powers compared to the hydrogen beam case.

Appendix I

THE JET TEAM

JET Joint Undertaking, Abingdon, Oxon, OX14 3EA, U.K.

J.M. Adams[1], B. Alper, H. Altmann, A. Andersen[14], P. Andrew, S.Ali-Arshad, W. Bailey, B. Balet, P. Barabaschi, Y. Baranov, P. Barker, R. Barnsley[2], M. Baronian, D.V. Bartlett, A.C. Bell, G. Benali, P. Bertoldi, E. Bertolini, V. Bhatnagar, A.J. Bickley, D. Bond, T. Bonicelli, S.J. Booth, G. Bosia, M. Botman, D. Boucher, P. Boucquey, M. Brandon, P. Breger, H. Brelen, W.J. Brewerton, H. Brinkschulte, T. Brown, M. Brusati, T. Budd, M. Bures, P. Burton, T. Businaro, P. Butcher, H. Buttgereit, C. Caldwell-Nichols, D.J. Campbell, D. Campling, P. Card, G. Celentano, C.D. Challis, A.V.Chankin[23], A. Cherubini, D. Chiron, J. Christiansen, P. Chuilon, R. Claesen, S. Clement, E. Clipsham, J.P. Coad, I.H. Coffey[24], A. Colton, M. Comiskey[4], S. Conroy, M. Cooke, S. Cooper, J.G. Cordey, W. Core, G. Corrigan, S. Corti, A.E. Costley, G. Cottrell, M. Cox[7], P. Crawley, O. Da Costa, N. Davies, S.J. Davies[7], H. de Blank, H. de Esch, L. de Kock, E. Deksnis, N. Deliyanakus, G.B. Denne-Hinnov, G. Deschamps, W.J. Dickson[19], K.J. Dietz, A. Dines, S.L. Dmitrenko, M. Dmitrieva[25], J. Dobbing, N. Dolgetta, S.E. Dorling, P.G. Doyle, D.F. Düchs, H. Duquenoy, A. Edwards, J. Ehrenberg, A. Ekedahl, T. Elevant[11], S.K. Erents[7], L.G. Eriksson, H. Fajemirokun[12], H. Falter, J. Freiling[15], C. Froger, P. Froissard, K. Fullard, M. Gadeberg, A. Galetsas, L. Galbiati, D. Gambier, M. Garribba, P. Gaze, R. Giannella, A. Gibson, R.D. Gill, A. Girard, A. Gondhalekar, D. Goodall[7], C. Gormezano, N.A. Gottardi, C. Gowers, B.J. Green, R. Haange, A. Haigh, C.J. Hancock, P.J. Harbour, N.C. Hawkes[7], N.P. Hawkes[1], P. Haynes[7], J.L. Hemmerich, T. Hender[7], J. Hoekzema, L. Horton, J. How, P.J. Howarth[5], M. Huart, T.P. Hughes[4], M. Huguet, F. Hurd, K. Ida[18], B. Ingram, M. Irving, J. Jacquinot, H. Jaeckel, J.F. Jaeger, G. Janeschitz, Z. Jankowicz[22], O.N. Jarvis, F. Jensen, E.M. Jones, L.P.D.F. Jones, T.T.C. Jones, J-F. Junger, F. Junique, A. Kaye, B.E. Keen, M. Keilhacker, W. Kerner, N.J. Kidd, R. Konig, A. Konstantellos, P. Kupschus, R. Lässer, J.R. Last, B. Laundy, L. Lauro-Taroni, K. Lawson[7], M. Lennholm, J. Lingertat[13], R.N. Litunovski, A. Loarte, R. Lobel, P. Lomas, M. Loughlin, C. Lowry, A.C. Maas[15], B. Macklin, C.F. Maggi[16], G. Magyar, V. Marchese, F. Marcus, J. Mart, D. Martin, E. Martin, R. Martin-Solis[8], P. Massmann, G. Matthews, H. McBryan, G. McCracken[7], P. Meriguet, P. Miele, S.F. Mills, P. Millward, E. Minardi[16], R. Mohanti[17], P.L. Mondino, A. Montvai[3], P. Morgan, H. Morsi, G. Murphy, F. Nave[27], S. Neudatchin[23], G. Newbert, M. Newman, P. Nielsen, P. Noll, W. Obert, D. O'Brien, J. O'Rourke, R. Ostrom, M. Ottaviani, S. Papastergiou, D. Pasini, B. Patel, A. Peacock, N. Peacock[7], R.J.M. Pearce, D. Pearson[12], J.F. Peng[26], R. Pepe de Silva, G. Perinic, C. Perry, M.A. Pick, J. Plancoulaine, J-P. Poffé, R. Pohlchen, F. Porcelli, L. Porte[19], R. Prentice, S. Puppin, S. Putvinskii[23], G. Radford[9], T. Raimondi, M.C. Ramos de Andrade, M. Rapisarda[29], P-H. Rebut, R. Reichle, S. Richards, E. Righi, F. Rimini, A. Rolfe, R.T. Ross, L. Rossi, R. Russ, H.C. Sack, G. Sadler, G. Saibene, J.L. Salanave, G. Sanazzaro, A. Santagiustina, R. Sartori, C. Sborchia, P. Schild, M. Schmid, G. Schmidt[6], H. Schroepf, B. Schunke, S.M. Scott, A. Sibley, R. Simonini, A.C.C. Sips, P. Smeulders, R. Smith, M. Stamp, P. Stangeby[20], D.F. Start, C.A. Steed, D. Stork, P.E. Stott, P. Stubberfield, D. Summers, H. Summers[19], L. Svensson, J.A. Tagle[21], A. Tanga, A. Taroni, C. Terella, A. Tesini, P.R. Thomas, E. Thompson, K. Thomsen, P. Trevalion, B. Tubbing, F. Tibone, H. van der Beken, G. Vlases, M. von Hellermann, T. Wade, C. Walker, D. Ward, M.L. Watkins, M.J. Watson, S. Weber[10], J. Wesson, T.J. Wijnands, J. Wilks, D. Wilson, T. Winkel, R. Wolf, D. Wong, C. Woodward, M. Wykes, I.D. Young, L. Zannelli, A. Zolfaghari[28], G. Zullo, W. Zwingmann.

PERMANENT ADDRESSES

1. UKAEA, Harwell, Didcot, Oxon, UK.
2. University of Leicester, Leicester, UK.
3. Central Research Institute for Physics, Budapest, Hungary.
4. University of Essex, Colchester, UK.
5. University of Birmingham, Birmingham, UK.
6. Princeton Plasma Physics Laboratory, New Jersey, USA.
7. UKAEA Culham Laboratory, Abingdon, Oxon, UK.
8. Universidad Complutense de Madrid, Spain.
9. Institute of Mathematics, University of Oxford, UK.
10. Freien Universität, Berlin, F.R.G.
11. Royal Institute of Technology, Stockholm, Sweden.
12. Imperial College, University of London, UK.
13. Max Planck Institut für Plasmaphysik, Garching, FRG.
14. Risø National Laboratory, Denmark.
15. FOM Instituut voor Plasmafysica, Nieuwegein, The Netherlands.
16. Dipartimento di Fisica, University of Milan, Milano, Italy.
17. North Carolina State University, Raleigh, NC, USA
18. National Institute for Fusion Science, Nagoya, Japan.
19. University of Strathclyde, 107 Rottenrow, Glasgow, UK.
20. Institute for Aerospace Studies, University of Toronto, Ontario, Canada.
21. CIEMAT, Madrid, Spain.
22. Institute for Nuclear Studies, Otwock-Swierk, Poland.
23. Kurchatov Institute of Atomic Energy, Moscow, USSR
24. Queens University, Belfast, UK.
25. Keldysh Institute of Applied Mathematics, Moscow, USSR.
26. Institute of Plasma Physics, Academica Sinica, Hefei, P. R. China.
27. LNETI, Savacem, Portugal.
28. Plasma Fusion Center, M.I.T., Boston, USA.
29. ENEA, Frascati, Italy.

At 1st July, 1992